

HETEROGENEOUS ORGANIC ACID UPTAKE ON SOOT SURFACES

A Thesis

by

NICHOLAS PAUL LEVITT

Submitted to the Office of Graduate Studies of
Texas A&M University
in partial fulfillment of the requirements for the degree of

MASTER OF SCIENCE

May 2007

Major Subject: Atmospheric Sciences

HETEROGENEOUS ORGANIC ACID UPTAKE ON SOOT SURFACES

A Thesis

by

NICHOLAS PAUL LEVITT

Submitted to the Office of Graduate Studies of
Texas A&M University
in partial fulfillment of the requirements for the degree of

MASTER OF SCIENCE

Approved by:

Chair of Committee,	Renyi Zhang
Committee Members,	Sarah Brooks
	Simon North
Head of Department	Richard Orville

May 2007

Major Subject: Atmospheric Sciences

ABSTRACT

Heterogeneous Organic Acid Uptake on Soot Surfaces. (May 2007)

Nicholas Paul Levitt, B.S., Texas A&M University

Chair of Advisory Committee: Dr. Renyi Zhang

Atmospheric particulates have been known to act as cloud condensation nuclei (CCN) and therefore their presence can indirectly affect important processes such as global radiation balance through cloud formation. Soot particles are well known to be atmospheric constituents, but the hydrophobic nature of fresh soot likely prohibits them from encouraging cloud development. Soot aged through contact with oxygenated organic compounds may become hydrophilic enough to promote water uptake. In this study I have observed the interaction between a number of carboxylic acids and soot from different fuel sources and formation mechanisms. A low pressure fast flow reactor was used to control the contact between the solid phase soot and gas phase organics, while chemical ionization-mass spectrometry was utilized to monitor concentrations of gas phase organics. Most acids irreversibly deposited on the soot surfaces, and the uptake coefficient was measured in the wide range of 9.0×10^{-4} to 1.0×10^{-1} . The Brunauer, Emmett, and Teller (BET) surface areas of the soots were measured and the soot bulk and surface chemical compositions were investigated with Fourier transform infrared (FTIR) spectroscopy and attenuated total reflection (ATR) spectroscopy to help explain differences in uptake. By comparing the mono and dicarboxylic acids and the information gathered from soot physiochemical properties I have discussed possible uptake mechanisms.

DEDICATION

I would like to dedicate this document to my grandparents, Jack Robert and Dorthea Kay Levitt, whose strong belief in education has inspired and enabled me to accomplish more than I could have imagined.

ACKNOWLEDGEMENTS

I would like to thank my committee chair, Dr. Renyi Zhang, for teaching me how to use my knowledge of chemistry to expand the horizons of human understanding. I would also like to thank my committee members, Dr. Sarah Brooks and Dr. Simon North, for useful discussions, wonderful teaching ability, and general advising assistance.

The funding for this work has been supplied by the Robert A Welch Foundation (Grant A-1417) and the US Environmental Protection Agency EPA (R03-0132) and is thankfully acknowledged.

I would like to show special appreciation toward Jun Zhao for helping me “learn the ropes” and Alexei Khalizov for sharing his world of knowledge with me; sometimes more than I asked for. I am also grateful for the assistance, comments, and suggestions from the rest of Dr. Zhang’s research group. Our time together has been a great experience for me.

The Laboratory for Molecular Simulation and Lisa Perez are gratefully acknowledged for opening a whole new branch of chemistry to me.

Finally, I want to recognize my friends and family for their unfailing support and patience.

NOMENCLATURE

A/F	Air to Fuel
ATR	Attenuated Total Reflection Spectroscopy
BC	Black Carbon
BET	Brunauer, Emmett, and Teller
C	Carbon or Celsius
CCN	Cloud Condensation Nuclei
CDG	Capacitance Diaphragm Gauge
DFT	Density Functional Theory
EC	Elemental Carbon
FTIR	Fourier Transform Infrared Spectroscopy
ID	Inner Diameter
ID-CIMS	Ion Drift-Chemical Ionization Mass Spectrometry
IR	Infrared
LYP	Lee, Yang, and Parr
MCT	Mercury Cadmium Telluride
MIR	Medium Infrared
OD	Outer Diameter
PAH	Polycyclic Aromatic Hydrocarbon
SGI	Silicon Graphics, Inc.
STP	Standard Temperature and Pressure
TGS	Triglycine Sulfate
VOC	Volatile Organic Compound

TABLE OF CONTENTS

	Page
ABSTRACT.....	iii
DEDICATION.....	iv
ACKNOWLEDGEMENTS.....	v
NOMENCLATURE.....	vi
TABLE OF CONTENTS.....	vii
LIST OF TABLES.....	viii
LIST OF FIGURES.....	ix
1. INTRODUCTION.....	1
2. EXPERIMENTAL.....	7
2.1. Uptake Measurements.....	7
2.2. Soot Chemical Characterization by FTIR and ATR Spectroscopy.....	12
2.3. BET Surface Area Measurements.....	13
2.4. Theoretical Calculations.....	17
3. RESULTS AND DISCUSSION.....	20
3.1. Uptake of Organic Acids on Soot.....	20
3.2. Effect of Physical Properties on Uptake.....	32
4. CONCLUSIONS.....	57
REFERENCES AND NOTES.....	61
VITA.....	66

LIST OF TABLES

TABLE	Page
1 Organic Acids Investigated.....	6
2 Dicarboxylic Acid Interaction or Uptake Summary.....	21
3 Uptake Values by Exposure Number.....	26
4 BET Measured Soot Surface Areas.....	40
5 Estimated Organic Acid Coverage of Geometric Soot Surface.....	54

LIST OF FIGURES

FIGURE	Page
1 Diagram of Flow-Tube Setup.....	12
2 Diagram of Custom BET Flask.....	14
3 Temporal Profile of Maleic Acid with Temporary Exposure to 58 mg of Unactivated Kerosene Soot Over a 20 cm Length.....	18
4 Temporal Profile of Phthalic Acid with Temporary Exposure to 35 mg of Methane Soot Over a 20 cm Length.....	19
5 Temporal Profile of Benzoic Acid with Stepwise Exposure in 2.5 cm Increments to 15 mg of Methane Soot Over a 7.5 cm Length.....	24
6 Intensity of Acid Signal as a Function of Injector Distance.....	25
7 Comparison of Uptake Coefficients as a Function of Exposure Number for Steric Acid Uptake on Different Amounts of Activated Propane Soot.....	29
8 IR Spectra of Propane Soot Deposited on ZnSe Crystal Plates.....	30
9 ATR and FTIR Spectra of Kerosene Soot.....	31
10 FTIR Spectra of Methane Soot Deposited on ZnSe Crystal Plates.....	33
11 Baseline Corrected Spectra of Activated Kerosene Soot Collected by ATR (Blue), Activated Propane Soot (Red), and Methane Soot (Green).....	34
12 Adsorption Isotherm of Kr on 0.0144 g of Unactivated Kerosene Soot at 77.5 K.....	38
13 BET Plot of $P/V(P_0 - P)$ Against P/P_0	39
14 Uptake Coefficients as a Function of Exposure Number for Benzoic Acid Uptake on Kerosene Soot.....	43
15 Uptake Coefficients as a Function of Exposure Number for Steric Acid Uptake on Kerosene Soot.....	44

FIGURE	Page
16 Uptake Coefficient as a Function of Exposure Number for Oleic Acid Uptake on Propane Soot.....	45
17 Uptake Coefficient as a Function of Exposure Number for Steric Acid Uptake on Propane Soot.....	46
18 Uptake Coefficients Are Displayed as a Function of Exposure Number for Steric Acid Uptake on Methane Soot.....	47
19 Theoretically Optimized Benzoic Acid Structure.....	50
20 Theoretically Optimized Steric Acid Structure.....	51
21 Theoretically Optimized Oleic Acid Structure.....	52
22 Cartoon Representation of Spherical Soot Sub-Particles and Organic Acids to Give an Idea of Scale.....	53

1. INTRODUCTION*

Aerosols play a vital role in many atmospheric processes. They have been shown to directly affect radiation balance through reflection or scattering of visible light and absorbing infrared energy.¹ Atmospheric particulate matter is also capable of promoting cloud formation and thus also indirectly playing a role in radiation balance.² These phenomena can cause aerosols to impact global climate on a larger time scale.³ Aerosols have also been shown to be detrimental to human health, air quality, and visibility.⁴ Soot, a form of black carbon (BC), is one type of atmospheric aerosol that is of special concern because of the uncertainty surrounding its involvement in the aforementioned processes. Soot is the result of incomplete hydrocarbon combustion and has a global emission rate of up to 24 Tg yr⁻¹.⁵ Schultz reports black carbon as being ~20% of the total particulate matter in the 3-48 μm range in Berlin⁶ and Gray et al. report 14.9% of all fine aerosols are elemental carbon in the Los Angeles sky⁷ while Kaneyasu and Murayama have measured black carbon concentrations over 150 ng C m⁻³ above the central Pacific Ocean.⁸

This thesis follows the style of the *Journal of Physical Chemistry A*.

*Reproduced with permission from *Journal of Physical Chemistry A*, Submitted for Publication. Unpublished work copyright, 2007, American Chemical Society.

Carbon has a long history of industrial use, and carbon from soot has played a major role in processes such as pigment and rubber production.⁹ Soot collected from unobstructed but oxygen deficient flames of oils and gasses is referred to as lampblack¹⁰ while soot deposited on a surface in an impinging manner is termed channel black.¹¹ Soot can also be used as a source for activated carbon, but the process of activation by heating and oxidation by steam or carbon dioxide is required to increase surface area to the 500-1400 m² g⁻¹ required for this material.⁹ However, materials such as coal, nut shells, lignite, wood, and pulp mill residue have been shown to be superior to soot as activated carbon precursors so it is almost never used for that purpose and converts better to materials such as graphite. Some studies have been conducted on raw soot to determine its adsorption capabilities. Beebe et al. report monolayer heats of adsorption in the 5 to 9 kcal mol⁻¹ range for C4-C5 alkanes and alkenes on commercial channel black samples.^{12,13} A study by Tesner and Polyakova reports that benzene adsorption is highest on channel black, medium on acetylene soot, and low on lampblack. The study goes on to report a Type II adsorption isotherm for methanol on channel black, but a Type III isotherm for the same alcohol on acetylene soot.¹⁴ Pidgeon has found that sorption of methylene blue and iodine increases as the height of a channel above a hydrocarbon (C1-C4) flame increases.¹⁵ A good review of how raw soots can be chemically altered changing adsorptive properties is given by Avgul and Kiselev.¹⁶

The fate of soot in the atmosphere depends on its level of ageing. Soot that has been oxidized or coated may interact with water in the atmosphere and follow wet deposition pathways rather than dry deposition that its hydrophobic nature would

otherwise necessitate. One class of organic species relevant to the atmosphere and possibly able to interact with soot is organic acids. Organic acids are produced from oxidation of volatile organic compounds (VOCs) as well as from biomass and fuel burning.¹⁷⁻²⁰ Larger fatty acids can enter the atmosphere after being shed by plant and animal material or through anthropogenic processes such as grilling and frying.²¹⁻²⁷

A wide variety of experimentation and field monitoring has been done to better understand the role of soot in the atmosphere. In addition to the annual emission rate and concentrations, many physical properties of soot have been investigated. Soot formation is understood to occur after pyrolysis of hydrocarbons where ionic carbon atoms or molecule fragments recombine to form aromatic and polyaromatic structures. Mansurov explains in a recent review²⁸ that these conjugated systems continue to assemble in continuous graphite-like sheets until the structures are large enough to condense. After particles are formed they continue to grow through surface deposition and finally coagulation and aggregation. Some types of BC and elemental carbon (EC) can have a highly ordered crystalline structure, but soot is usually much less ordered and commonly amorphous.²⁹ Soot particles can grow up to a few micrometers in length.³⁰ The resulting soot particles possess large porosities and significant internal surface areas. Passages between pores tend to resemble nanotubes with micro and mesopores forming among spherical elementary particles.³¹ Soot formation is critically sensitive to the conditions in which it is produced.³² Temperature, pressure, air mixing ratio, pyrolysis initiation method, and many other factors can all change the resulting soot circumstances. Elemental makeup of soot is between 80-100% carbon depending on the fuel, with the

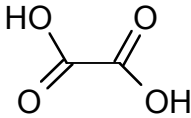
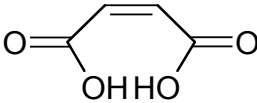
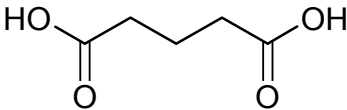
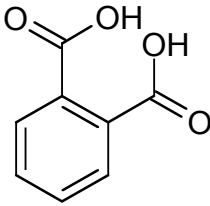
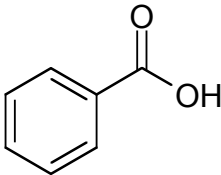
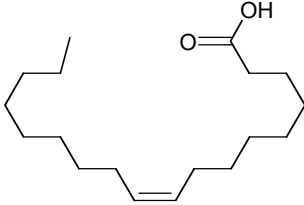
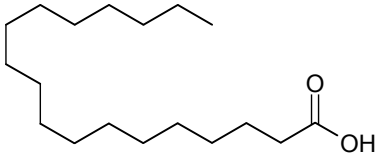
balance consisting of mainly hydrogen and oxygen with the possibility of some nitrogen and sulfur.^{33,34} Soot has a tremendous ability to absorb solar and terrestrial radiation, but factors such as soot coating by organics and changes in absorption cross section can dramatically change absorption and single scattering albedo of the soot.^{35,36} The better these properties and interaction consequences are understood, the more effectively modeling of aerosol microphysics and cloud/climate interaction will be.

Much attention has been paid to soot aging and interaction with atmospheric gas phase species recently.^{31,37-40} These studies have focused on the aging of soot as it relates its ability to be cloud condensation nuclei (CCN)⁴¹ and alteration of optical properties⁴² as well as the possible role soot could play in ice nucleation⁴³ or acting as a substrate for atmospheric reduction-oxidation reactions.⁴⁴ Small inorganic molecule adsorption to soot has been found by Chughtai et al. to be facilitated by high concentrations of unpaired electrons in soot infrastructure.⁴⁵ Uptake coefficients on soot have been measured for ozone,^{46,47} water,^{34,48} sulfuric acid,⁴¹ nitric acid,^{47,49-51} nitrogen dioxide,⁵⁰⁻⁵³ and nitrogen pentoxide.⁴⁷ Similar studies have focused on organic uptake by other carbonaceous solid matter. These studies include polyaromatic hydrocarbon (PAH) uptake on coal fly ash,⁵⁴ PAH sorption by carbon nanomaterials,⁵⁵ and benzene derivatives and cyclohexane on wood charcoals.⁵⁶ The uptake experiments record a range of coefficients varying by orders of magnitude. Generally, as soot becomes aged, the tendency for gas phase species to adsorb to the surface will decrease. Gas phase concentrations and soot types also play a role in heterogeneous partitioning, but the biggest factor determining uptake seems to be the adsorbate itself. To date, it is the

understanding of the author that only one optical study of an organic acid and soot interaction⁵⁷ has been published. A better working knowledge of the interaction between soot particles and organic acids is necessary to understand how soot impact on atmospheric parameters and conditions changes as it is aged by these species.

In this work I have studied the interaction between several monocarboxylic and dicarboxylic acids and soots formed by combustion of methane, propane, and kerosene. Soot was deposited by either allowing the flame to come into contact with the deposition surface (activated) similar to industrial channel black or by positioning the deposition substrate well above the flame level (unactivated) as in lampblack processes. It is important to point out that “activated” here does not denote the same activation process used to form activated carbon, but rather an attempt to follow nomenclature convention used by Aubin and Abbatt.⁴⁴ Monocarboxylic acids used in this study were benzoic, steric, and oleic while dicarboxylic acids included oxalic, maleic, glutaric, and phthalic. For monocarboxylic acids that exhibited irreversible loss on soot, the uptake coefficient was measured several times sequentially in order to gauge the aging affect on uptake. For comparison reasons, dicarboxylic acid uptake coefficients were assessed for initial uptake. Optimized monocarboxylic acid structures were theoretically determined to appraise molecular dimensions and orientations. Physical and chemical properties of the soot samples were investigated to help explain differences in uptake and uptake magnitude for different organic acid/soot combinations. BET isotherms were performed to evaluate soot surface areas while FTIR and ATR-FTIR spectroscopy was utilized to gauge the level of functional group availability inside and on the surface of the soot.

Table 1. Organic Acids Investigated

Name	Formula	MW (g mol ⁻¹)	Structure
Oxalic Acid	C ₂ H ₂ O ₄	90.03	
Maleic Acid	C ₄ H ₄ O ₄	116.07	
Glutaric Acid	C ₅ H ₈ O ₄	132.11	
Phthalic Acid	C ₈ H ₆ O ₄	166.13	
Benzoic Acid	C ₇ H ₆ O ₂	122.12	
Oleic Acid	C ₁₈ H ₃₄ O ₂	282.46	
Steric Acid	C ₁₈ H ₃₆ O ₂	284.48	

2. EXPERIMENTAL

2.1. Uptake Measurements

The uptake measurements were performed using a low-pressure laminar flow reactor in conjunction with ion drift – chemical ionization mass spectrometry (ID-CIMS) detection, similar to work described previously.⁵⁸⁻⁶⁰ A Pyrex reactor of 70 cm in length and internal radius of 1 cm was used. In the reactor a slightly smaller glass tube (20 cm long and with an internal radius of 0.8 cm) with soot coating the inside walls was placed.

Benzoic acid (Fisher Scientific, 99.5%), glutaric acid (Sigma, 99%), maleic acid (Sigma-Aldrich, 99%), oleic acid (Sigma, ~99%), oxalic acid (Aldrich, 98%), phthalic acid (Sigma-Aldrich, 99.5%), and steric acid (Sigma-Aldrich, 95%) were used as received without further purification. Table 1 shows atomic formulas, molecular weights, and structures of the organic acids used in this study. A sample bubbler containing the acid was placed in a temperature bath to regulate its concentration in the flow reactor. For benzoic acid, a room temperature water bath was used and for maleic acid, oxalic acid, and phthalic acid, the bath temperature was close to 100° C. The water bath for oleic acid and glutaric acid both ranged from about 83 to 89° C while the bath for steric acid ranged from 56 to 63° C. The acid purity was checked by ID-CIMS. The acid vapor was introduced into the flow reactor through a movable injector. Benzoic acid, glutaric acid, oleic acid and oxalic acid in the flow reactor were estimated to be on the order of 10^{-4} Torr. Steric acid was estimated to be on the order of 10^{-5} Torr while phthalic acid and maleic acid were estimated to be on the order of 10^{-6} Torr. All carrier flows were monitored with calibrated electronic mass flow meters (Millipore Tylan 260

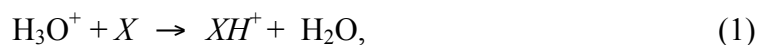
Series). The flow reactor was operated under the laminar flow conditions (i.e., the Reynold number $Re=2aup/\mu < 2000$, where a is the internal radius of the flow reactor in cm, ρ is the density of the gas in g cm^{-3} , u is the flow velocity in cm s^{-1} , and μ is the absolute viscosity of the gas) with a pressure of about 0.35 Torr and typical flow velocities of $500\text{--}800 \text{ cm s}^{-1}$.

Methane soot was obtained from burning gas from an in-house fuel source. Propane was obtained commercially in the gas-grill style tank. Kerosene was obtained from the Alfa Aesar Company. Fuels were used as purchased without further purification. Soot was deposited on the sample tube for approximately an hour at a time. For methane and propane, a commercial light-duty torch was used as a burner and a commercial alcohol burner was used to maintain the kerosene flame. During each coating process the flame was adjusted by altering the amount of fuel available to produce a “sooting” flame to speed up the deposition process. In most cases, this entailed closing the air entrance of the commercial torch so that no air mixed with the gas fuel before combustion and for the alcohol burner increasing the wick length and keeping the liquid kerosene level high. Jones et al. report that low air to fuel (A/F) ratios have a number of consequences. The results of this setup include smaller surface oxidation and decreased soot particle growth rates.⁶¹

The soot was applied in two different manners. The first process had the tube well above the tip of the flame so that the tube walls were never exposed to the flame. In the second process, the flame was allowed to exist inside the tube so that the fire came in contact with the wall due to the natural motion of the flame. In these two ways the

soot on the tube walls was made to be “unactivated” or “activated,” respectively. For the methane flame, combustion was sufficiently effective enough that soot was not deposited unless the “activated” method was employed. For this reason, only “activated” soot was used for methane experiments. Mass of soot deposited in the tube varied widely from fuel source to fuel source and between the two methods. Amounts of soot as small as a few milligrams and as large as 200 milligrams were deposited. The soot tube was replaced with a fresh sample for each new experiment and the amount of soot on the tube was measured after each experiment.

Details of the ID-CIMS instrumentation have been described previously.⁶² Briefly, the proton transfer reaction with H_3O^+ was used,



where X and XH^+ denote the organic acid species or its fragment and the corresponding protonated form, respectively. Maleic acid, oleic acid, phthalic acid, and steric acid were monitored at their protonated fragmentation peaks ($m/z=99$ for maleic acid, 169 for oleic acid, 149 for phthalic acid, and 145 for steric acid, respectively) for higher detection sensitivity. Maleic acid fragment peak was formed by protonation of the oxygen on the OH group and then loss of this group as a neutral water molecule. The molecular weight of maleic acid (116) minus the molecular weight of an OH group (17) would equal an m/z of 99. This same mechanism forms the fragment of phthalic acid and also mathematically works out to a give m/z of 149. Steric and oleic acid being larger molecules, the fragmentation mechanism is less clear. One possible fragmentation pattern for steric acid that would explain m/z 145 is bond rupture between the C9 and

C10 carbons and protonation of two of the three following locations on the larger fragment: either oxygen or the new terminal carbon. Similarly, to leave an m/z of 169 oleic acid would have to lose the last eight carbons and their respective hydrogens and again have either of the oxygens or the new terminal carbon protonated. Intensity of the fragment peak was observed to be linearly proportional to that of its parent acid flow tube concentration. Benzoic acid, glutaric acid, and oxalic acid were monitored at their protonated peaks ($m/z=$ 123 for benzoic acid, 133 for glutaric acid, and 91 for oxalic acid, respectively).

The interaction between all combinations of soots and acids were assessed by exposing the length of the soot tube to the flow of organic acid vapor. This was accomplished by retracting the moveable injector to a position upstream of the soot tube. A diagram of this setup is given in Figure 1. In the cases of irreversible loss, the signal dropped to a substantially lower level and did not increase significantly on the time scale of the experiment. The uptake coefficient (γ) was determined by monitoring the organic species as it was exposed to the soot. The uptake coefficient represents the ratio of successful gas-surface collisions to the sum of all gas-surface collisions. A successful collision was one in which the gas phase species was irreversibly removed from the gas phase. To calculate the uptake coefficient, the first-order rate constant (k) was measured by way of signal loss:⁶³⁻⁶⁵

$$\gamma = \frac{2rk}{\omega + rk} \quad (2)$$

where r is the radius of the flow reactor and ω is the mean thermal speed. The geometric inner surface area of the soot tube was used in these uptake coefficient

calculations. Gas phase diffusion correction was accomplished through the work by Brown.⁶⁶ This numerical algorithm allowed me to describe radial organic acid gradients in the reaction chamber due to significant reactive wall loss so the observed first -order reaction rate constant (k_{obs}) could be found. The gas-phase diffusion coefficients were estimated by the method described by Fuller et al.⁶⁷ with the improvements suggested by Marrero and Luecke.⁶⁸ The values used for steric acid, oleic acid and benzoic acid were 102.8, 103.8, and 193.9 Torr cm² s⁻¹, respectively. Dicarboxylic acid gas-phase diffusion coefficients were estimated to be 240.9, 178.9, and 167.1 Torr cm² s⁻¹, for oxalic, glutaric, and phthalic acid, respectively. Brown's correction proved to be fairly significant. For uptake coefficients up to 0.05, uptake was underestimated by 18 to 45% for steric acid. At $\gamma = 0.065$ the corrected value was 57% higher. Oleic acid corrections were not quite as impressive at 17 to 40% for uptake coefficients between 0.016 and 0.07. The highest uptake coefficients (~ 0.1) had only a deviation of 50%. For benzoic acid uptake coefficients, the uncorrected values were 17-40% off up to $\gamma = 0.008$, but only a 48% difference was found for an uptake coefficient of 0.017. Most dicarboxylic acid corrections were around 30% with the high being 42% and the low 22%. Corrections were most significant under conditions where k_{obs} approached the diffusion limited rate constant (k_d).

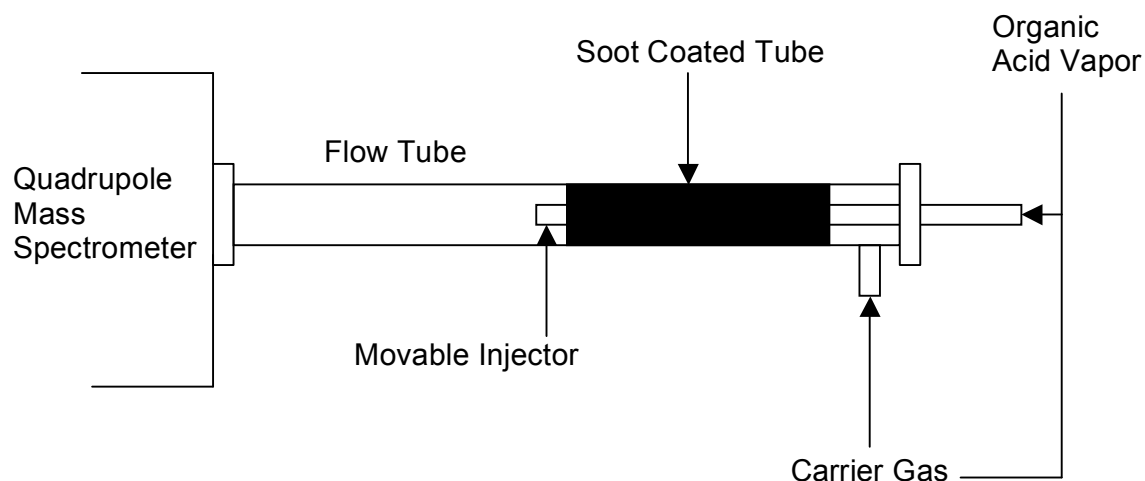


Figure 1. Diagram of flow-tube setup.

2.2. Soot Chemical Characterization by FTIR and ATR Spectroscopy

The chemical composition of the soot surface is of special interest in this study. To describe and attribute organic acid/surface interaction it is necessary to understand the structure at the soot surface and know what functional groups are available there. To investigate this property, I made use of FTIR and ATR Spectroscopy on deposited surfaces.

Soot was deposited on a ZnSe crystal plate in one of the two manners described in the previous section to either test “unactivated” or “activated” soot. The coating was thin (~ 1 mg) to prevent total absorbance of IR-light. A Nicolet Magna 560 spectrometer with MCT detector was used to measure spectra at 2 cm^{-1} resolution for the FTIR investigations. An average of 64 scans was used to collect spectra in a typical wavenumber range from 5000 to 750 cm^{-1} .

The ATR-FTIR instrument used in this study was a Perkin Elmer Spectrum 100 employing a MIR TGS detector. The crystal type used was ZnSe and had dimensions which were 1cm by 5cm and a penetration depth of $0.5\mu\text{-}5\mu$. ATR spectra were corrected for comparison to FTIR spectra after averaging a collection of 20 scans at resolution of 4 cm^{-1} over the typical wavenumber range from $4000\text{ to }750\text{ cm}^{-1}$. Soot was deposited on a single side of commercial aluminum foil in the manner described above in order to test “unactivated” or “activated” soot. The foil was cut to fit into the depression above the ATR crystal and allow efficient contact between the soot and crystal surface. The crystal was cleaned of all soot between experiments and blank samples confirmed the absence of absorbing material on the surface.

2.3. BET Surface Area Measurements

The porosity of the soot samples gives them a much larger surface area than their geometric shape would lead me to believe. The most common theory employed to measure surface area was developed by Brunauer et al.⁶⁹ and application of the theory has become known as the BET method after authors: Brunauer, Emmett, and Teller. Soot surface areas for n-hexane have been found to be 90-370 times larger than the geometric surface area occupied by the soot.⁴⁴ For this reason I have employed this technique to probe the relationship between “non-activation” and “activation” of soot and the resulting surface area.

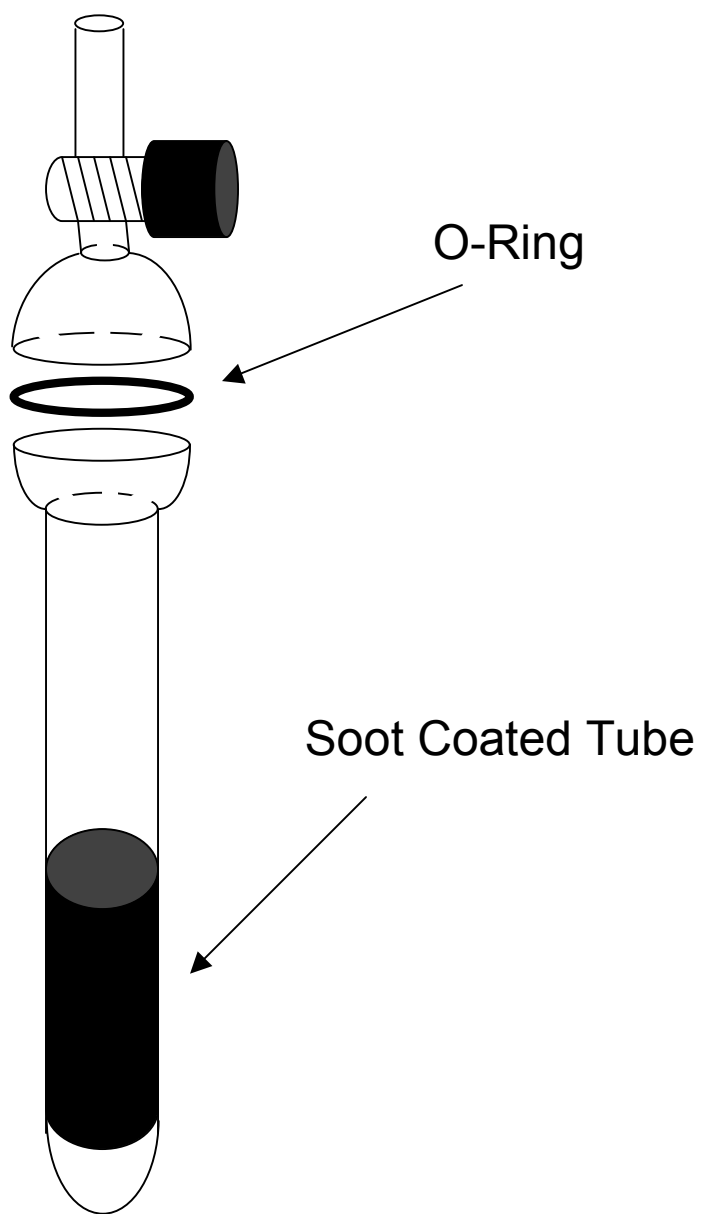


Figure 2. Diagram of custom BET flask.

The BET procedure involves using a specified gas to measure an adsorption isotherm at 77K. Research purity krypton was obtained from the Matheson Tri-Gas Company. The isotherm was constructed by placing a soot coated glass tube in a custom made glass flask with only one inlet. The glass tube was coated on the inside with either “unactivated” or “activated” soot and possessed the same internal radius (0.8 cm) but only half the length (10 cm) of the tubes used in the uptake experiments. Therefore the geometric surface area of the soot inside the tube was 50.24 cm^2 . The custom glass flask was much like a water bubbler (See Figure 2) insomuch that it had a long cylindrical bottom (for holding the soot tube and supplying efficient thermal contact) that ends near the top with a round glass joint. The top portion of the flask was merely a valved inlet sitting atop the complementary round glass joint. A Viton o-ring sealed the round glass joint which was necessary to allow the soot tube to be added or removed. The bottom portion measured 20 cm in length with an outer diameter (OD) of 2.6 cm and an inner diameter (ID) of 2 cm. The top of the flask totaled 14 cm in length, with 4 of those being the round glass joint. The inlet was $\frac{1}{4}$ ” tubing and ran parallel out from the center of the flask.

To effectively degas the soot sample, heating tape maintained a temperature of $\sim 473 \text{ K}$ for a minimum of 1 hour under vacuum in the uptake flask. Following heating, a period of approximately 20 minutes was used to allow cooling, also under vacuum. After flask cooling and during surface area measurement, the flask was submerged in liquid nitrogen so the soot surface was maintained at this temperature. Portions of Kr were subsequently added to the flask from a known initial volume while pressure was

monitored at each step. A Varian Ceramicel CDG baratron gauge was used to measure pressure in my system. The pressure in the flask was corrected for thermal transpiration in the manner suggested by Rosenberg,⁷⁰

$$P = P_m \left[1 - \frac{0.490}{37.2D^2 P_m^2 + 14.45DP_m + 1} \right] \quad (3)$$

where P is the corrected pressure in the flask, P_m is the pressure measured in the rest of the system by the baratron, and D is the diameter of the connection between the flask and the rest of the system. In this manner, it was possible to calculate the amount of Kr adsorbed by the soot surface from the known amount of krypton added, the known total volume of the system, and the change in pressures. The uptake of Kr and the surface area can be described by the BET equation,⁷¹

$$\frac{P}{V(P_0 - P)} = \frac{1}{V_m C} + \frac{P(C - 1)}{V_m C P_0} \quad (4)$$

where P_0 is the saturation vapor pressure of the Kr, V is the adsorbed volume in units of cubic centimeters at standard temperature and pressure (STP), V_m is the volume of the monolayer capacity also at STP, and C is the BET constant which has no units. Manipulation of this equation will allow $P/[V(P_0 - P)]$ to be plotted against P/P_0 which will yield a linear relationship.⁷² From a linear fit of this plot, the BET constant and the monolayer capacity can be extracted. The value of C is $1 + \text{slope}/\text{intercept}$ and V_m is $1/(\text{slope} + \text{intercept})$. The total surface area (SA_{BET}) of the soot being measured was calculated by,

$$SA_{\text{BET}} = V_m N_A \sigma_{\text{Kr}} \quad (5)$$

where V_m was the monolayer capacity converted to moles, N_A is Avogadro's number, and σ_{Kr} was the atomic cross-sectional area of Kr. The Kr saturation vapor pressure value used at 77K was 2.49 Torr⁷³ and molecular area of Kr was taken to be 20.2 Å².⁷⁴

2.4. Theoretical Calculations

A SGI Origin 3800 Supercomputer in conjunction with the GAUSSIAN 03 software package was employed to make all theoretical calculations. The level of Density Functional Theory (DFT) used in this study was Becke's three-parameter hybrid method. The LYP correction function was also considered giving (B3LYP) total theory. The mathematical restriction of the molecular orbitals, or basis set, used was a split valence polarized basis set. The d and p orbital functions have been added for a basis set of 6-31G(d,p) or 6-31G**.

The monocarboxylic acid structure geometries were optimized to find the lowest energy configuration. Monocarboxylic acids were chosen because their structures were three of the four largest and most complex of the carboxylic acids investigated and their uptake was also more extensively studied than that of dicarboxylic acids. From the resulting structures the molecular dimensions and positions of carboxylic groups were found. This information was also valuable in the assessment of uptake mechanism and other soot-organic acid interaction processes.

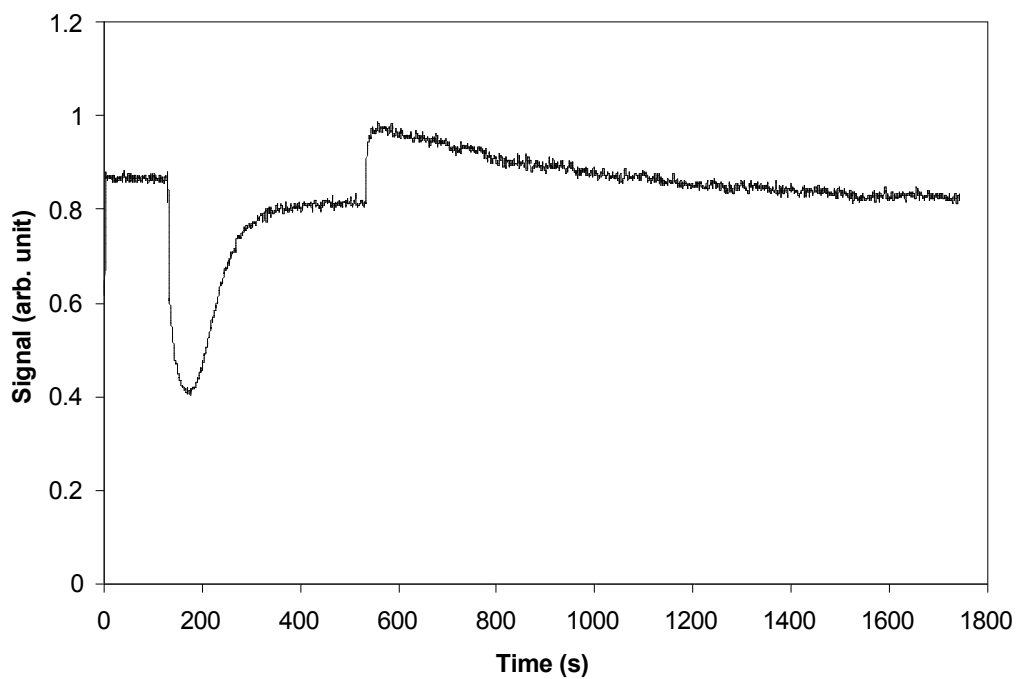


Figure 3. Temporal profile of maleic acid with temporary exposure to 58 mg of unactivated kerosene soot over a 20 cm length. The exposure was terminated after 500s.

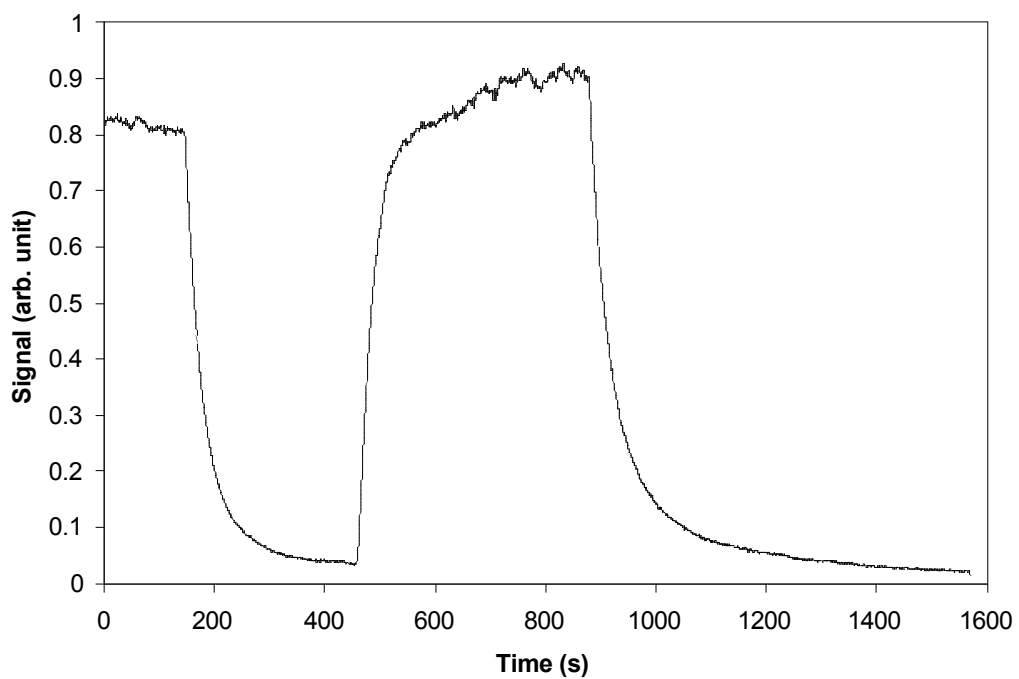


Figure 4. Temporal profile of phthalic acid with temporary exposure to 35 mg of methane soot over a 20 cm length. The phthalic acid flow was terminated after 900 s.

3. RESULTS AND DISCUSSION

3.1. Uptake of Organic Acids on Soot

Uptake measurements were performed by exposing a certain length of the soot to the organic acid vapor, while monitoring the organic acid signal using the ID-CIMS. For a few cases, the uptake of the organic acid on certain types of soot proved to be reversible. This can be seen in Figure 3 where the maleic acid signal dropped immediately upon exposure to a 20 cm length of unactivated kerosene soot, but quickly recovered and stabilized near the level of the original signal. After moving the injector and organic acid addition downstream of the soot, an increase in signal indicates organic acid leaving the soot and thus increasing the gas phase concentration. The recoverable adsorption curve was not identical to that of desorption, but an estimation of the area above the adsorption curve and the area below the desorption curve suggests all the maleic acid that was taken up by the soot was also given off.

For most cases uptake was irreversible and adsorption to the solid soot was evident from the sharp decline in the organic acid signal. Figure 4 shows temporal profiles of phthalic acid as it was exposed and later bypassed a 20 cm length of methane soot. The phthalic acid concentration in the gas phase dropped instantly upon exposure to the soot and returned to approximately its original value after the exposure was terminated. At 900 seconds into the experiment, the phthalic acid bubbler was bypassed to monitor the background for this species. The level at which the background stabilized was the same as that of the phthalic acid being exposed to the methane soot. This

indicates that strong uptake along the full length of the soot tube almost entirely depleted the organic acid from the gas flow.

Table 2. Dicarboxylic Acid Interaction or Uptake^a Summary

Soot Type			Methane	Propane		Kerosene	
				Unactivated	Activated	Unactivated	Activated
Acid	# C ^b	#DB ^c	$\gamma(10^{-2})$	$\gamma(10^{-2})$	$\gamma(10^{-2})$	$\gamma(10^{-2})$	$\gamma(10^{-2})$
Oxalic	2	0	0.09±0.01	None	0.17±0.02	0.18±0.10	0.18±0.05
Maleic	4	1	Reversible	None	Rev & Irrev	Reversible	Reversible
Glutaric	5	0	0.59±0.12	Reversible	0.37±0.12	0.42±0.12	0.46±0.06
Phthalic	Aromatic		0.76±0.26	0.38±0.07	0.65±0.24	0.57±0.01	0.77±0.47

^a Uptake coefficient values represent averages of at least two experiments.

Error corresponds to second standard deviation (σ^2).

^b Number of carbon atoms in molecule.

^c Number of double bonds in molecule.

The interactions observed for dicarboxylic acids in this study are summarized in Table 2. Uptake coefficient values indicate irreversible uptake. Behavior for the combination of maleic acid and “activated” propane soot was not consistent, so the uptake cannot be considered fully reversible or fully irreversible. Using unactivated propane soot under my conditions no significant interaction or uptake was observed for oxalic acid or maleic acid, and glutaric acid uptake was reversible. Also included in the table are the number of carbons in the organic acid carbon chain and the number of double bonds in that chain. Phthalic acid is an aromatic ring with two adjacent carboxylic acid groups bonded to the ring. The length of the carbon chain and its level of saturation may play a role in its ability to be taken up by soot. Aubin and Abbatt have shown for aromatic gasses that the magnitude of adsorption enthalpies increases as conjugation and molecule complexity increases.³⁷ This trend has been linked to the

vapor pressure of the organic and was possible due to increasing ability to hydrogen bond and to have van der Waals interactions with the soot. These findings are supported by a recent theoretical study by Kubicki³⁸ that shows interaction between PAHs and soot was due mainly to π - π system van der Waals forces. These calculations also go on to show that larger and more aromatic molecules will have a higher attraction to soot. The observation that maleic acid, with one carbon-carbon π system, had little or no irreversible uptake on the soots studied here while the other organic acids with no carbon-carbon π -bonds had uptake seems strange in light of the evidence presented by Aubin, Abbatt, and Kubicki. One possible explanation for this is that the interaction between maleic acid and soot was due to the reversible π - π system van der Waals forces and the irreversible interaction between the other dicarboxylic acids and soot was due to different attractive or reactive mechanisms of their oxygenated functional groups. Possible products from heterogeneous reactions between gas phase organic acids and soot or soot constituents entering the gas phase were not detected during uptake experiments for any combination except for oleic acid on activated kerosene soot. For this reason, it is not likely that organic acid molecules were reacting or dissociating on the soot surface and then re-entering the gas phase. For the case that a possible gas phase reaction product or product fragment was detected for oleic acid on activated kerosene soot at m/z 181, a likely reaction mechanism is not obvious. The increase at m/z 181 did correspond to exposure to the soot, but simultaneous oleic acid uptake behavior was erratic and inconsistent. More investigation is necessary to understand the interaction between oleic acid and activated kerosene soot.

For the three monocarboxylic acids studied, most interactions were also irreversible. The exceptions were benzoic acid on “unactivated” propane and oleic acid on “activated” kerosene soot. For benzoic acid, the uptake was reversible while oleic acid showed inconsistent uptake much like maleic acid on activated propane. Additional experiments were performed to obtain the uptake coefficients for the monocarboxylic acids that showed clear irreversible uptake. Figure 5 demonstrates the loss of benzoic acid as a function of the injector position when the injector was withdrawn at a 2.5 cm length interval. Decays followed the pseudo-first order kinetics. The pseudo-first order rate constant was determined from the slope of the linear least square fit of the data shown in Figure 6. This slope is one of the parameters used in the Brown method described above. The uptake coefficients were thus computed from the obtained pseudo-first order rate constant.

Dicarboxylic acids were used in this investigation to help look into the uptake mechanism. Therefore the uptake coefficient values listed in Table 2 are measurements of the initial uptake. These uptake values help determine if the carbon chain (or ring) of the monocarboxylic acids was primarily responsible for uptake on soot due to hydrogen bonding and van der Waals interactions as well as the π - π system van der Waals forces of the unsaturated bonds in oleic acid and benzoic acid. These attractive forces likely contribute to uptake but cannot be solely attributable in light of uptake of small dicarboxylic acids. More likely the carbon systems as well as the oxygenated functional groups were both involved in the hydrogen bonding and van der Waals forces (including the π - π system interactions). As pointed out previously, the bonding associated with

unoxxygenated hydrocarbons has been shown to be reversible, so oxygen functionality interactions with soot may cause carboxylic acids to be more irreversible. In the reversible case of benzoic acid on unactivated propane soot and oleic acid on activated kerosene soot, the reversible uptake may be winning out over irreversible interactions involved with oxygen. Further investigation is necessary to elucidate just how oxygenated functional groups facilitate irreversible uptake as compared to reversible interactions associated with unoxxygenated hydrocarbons.

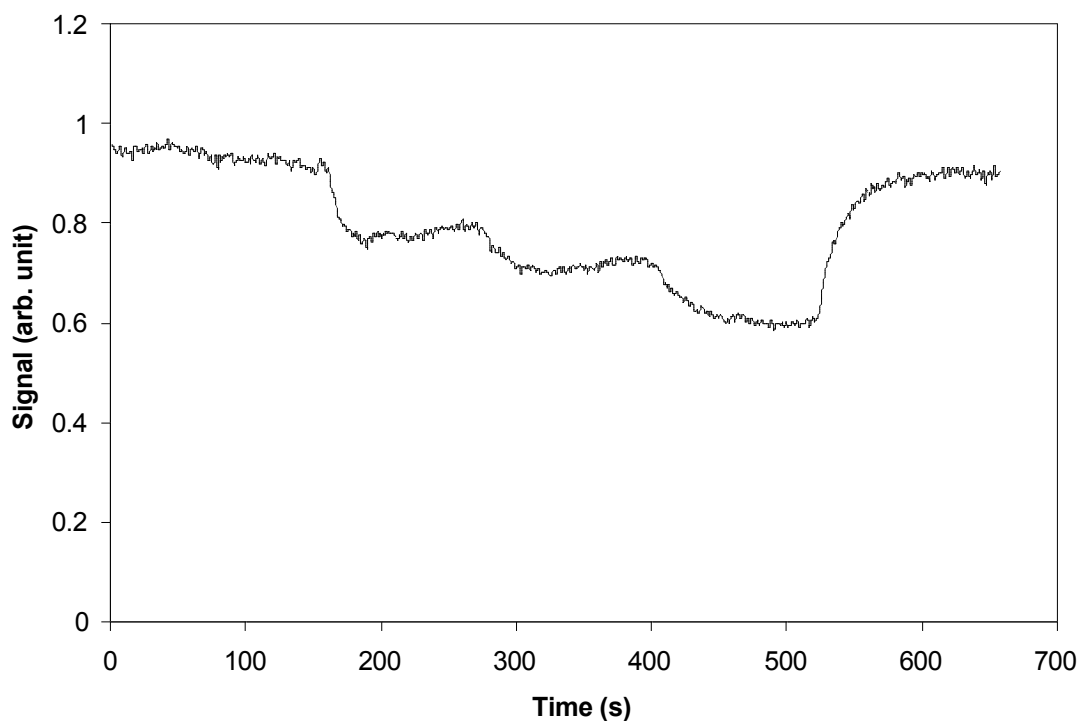


Figure 5. Temporal profile of benzoic acid with stepwise exposure in 2.5 cm increments to 15 mg of methane soot over a 7.5 cm length. Experimental conditions were $T = 296$ K, $P = 0.29$ Torr, and $u = 344$ cm s⁻¹. The injector was returned to its original position after 500 s.

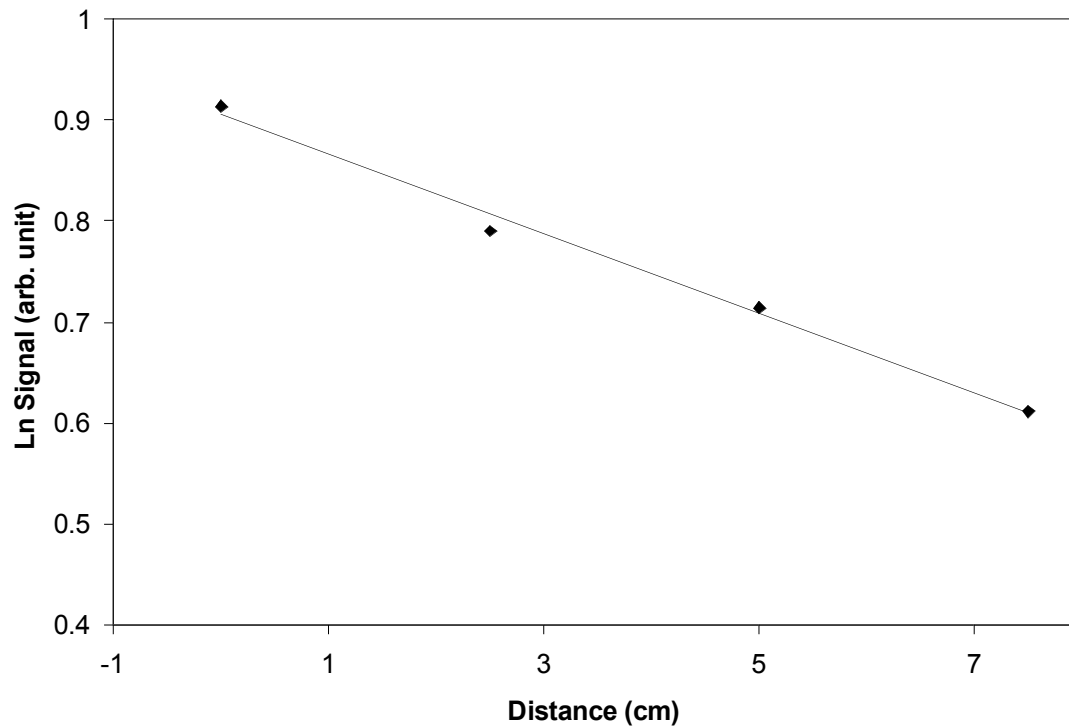


Figure 6. Intensity of acid signal as a function of injector distance. Solid diamonds identify benzoic acid data taken from the experiment described in Figure 3a.

Table 3. Uptake Values by Exposure Number^a

	Stearic Acid			Oleic Acid			Benzoic Acid		
	Exp. #	γ (10^{-2})	Dev. (10^{-2})	Exp. #	γ (10^{-2})	Dev. (10^{-2})	Exp. #	γ (10^{-2})	Dev. (10^{-2})
Methane Soot	1	0.98	0.45	1	0.95	0.38	1	0.21	0.07
	2	0.70	0.27	2	0.59	0.18	2	0.17	0.03
	3	0.53	0.26	3	0.48	0.08	3	0.16	0.04
	4	0.44	0.16	4	0.46	0.02	4	0.16	0.04
	5	0.34	0.12	5	0.48	0.04	5	0.16	0.04
	6	0.28	0.07	6	0.44	0.03	6	0.14	0.03
	mass	8 ± 5 mg		mass	8 ± 6 mg		mass	9 ± 5 mg	
Un-Activated Propane Soot	1	3.43	0.99	1	5.84	0.86	1	n/a	n/a
	2	2.32	1.19	2	5.25	1.26	2	n/a	n/a
	3	1.43	0.75	3	4.13	1.47	3	n/a	n/a
	4	0.98	0.50	4	3.51	1.30	4	n/a	n/a
	5	0.63	0.32	5	3.18	1.06	5	n/a	n/a
	6	0.43	0.26	6	3.22	0.93	6	n/a	n/a
	mass	3 ± 1 mg		mass	12 ± 1 mg		mass	n/a	
Activated Propane Soot	1	3.54	1.11	1	10.05	1.27	1	0.98	0.36
	2	2.67	0.81	2	8.75	1.03	2	0.94	0.49
	3	2.58	0.77	3	8.03	1.37	3	0.55	0.21
	4	2.12	0.70	4	6.91	2.06	4	0.43	0.12
	5	1.58	0.40	5	5.91	1.25	5	0.35	0.07
	6	1.23	0.39	6	5.18	0.68	6	0.30	0.09
	mass	25 ± 14 mg		mass	20 ± 10 mg		mass	31 ± 8 mg	
Un-Activated Kerosene Soot	1	5.03	1.23	1	4.44	1.18	1	1.74	0.37
	2	4.10	1.10	2	3.61	1.52	2	0.95	0.16
	3	3.47	1.13	3	2.75	1.43	3	0.79	0.34
	4	3.06	1.11	4	3.25	1.88	4	0.77	0.29
	5	3.01	0.95	5	2.91	2.05	5	0.47	0.20
	6	2.72	0.96	6	2.56	1.97	n/a	n/a	n/a
	mass	36 ± 18 mg		mass	13 ± 14 mg		mass	6 ± 1 mg	
Activated Kerosene Soot	1	5.36	2.05	1	n/a	n/a	1	1.33	0.83
	2	4.90	2.54	2	n/a	n/a	2	0.79	0.71
	3	3.59	1.68	3	n/a	n/a	3	0.57	0.39
	4	3.16	2.00	4	n/a	n/a	4	0.59	0.44
	5	2.74	1.62	5	n/a	n/a	5	0.51	0.30
	6	1.88	1.20	6	n/a	n/a	6	0.63	0.49
	mass	41 ± 11 mg		mass	n/a		mass	42 ± 27 mg	

^a At least three uptake sequences were used to average uptake values and masses. Error corresponds to second standard deviation (σ^2).

While the measurements of the dicarboxylic acids were not as extensive as those of the monocarboxylic acids, information past the uptake mechanism can be gleaned. Not considering the anomalous maleic acid, uptake tended to increase as the dicarboxylic acids increase in carbon number. This is consistent with Aubin, Abbatt, and Kubicki's findings that larger or more aromatic molecules were more attracted to soot.^{37,38} Uptake values can also be compared between the mono and dicarboxylic acids. Dicarboxylic acid uptake in general was on the order of monocarboxylic acid uptake on methane soot or that of benzoic acid. Some differences were noticed in the initial uptake between the two most structurally similar mono and dicarboxylic acids; benzoic and phthalic. The most important of these is that phthalic acid was irreversibly taken up by unactivated propane soot while benzoic acid was not. This also suggests that the oxygenated functional group aids in irreversible uptake.

The uptake of the monocarboxylic acids was observed to depend heavily on the duration of previous exposure. For this reason, stepwise experiments were sequentially performed on one soot sample to measure the decrease in uptake coefficient over time. One uptake experiment lasted approximately 250-450 seconds, so after 6 experiments the soot had been exposed for roughly 35 minutes. Table 3 lists the average uptake coefficients for the experiments of each organic acid and soot type combination. The table also showcases the previous exposure dependence by cataloging subsequent exposures to the soot. The mass listed for each combination was the average mass of the soot samples used for those experiments. In some cases, uptake values on the sixth exposure had only half the value as those on the first. For example, initial oleic acid loss

to methane soot was $\gamma = 0.95 \times 10^{-2}$ which decreased to $\gamma = 0.44 \times 10^{-2}$ for the sixth exposure. A trend was not evident from the table between the average mass used and range of uptake over exposures as might be expected. For example, it might be speculated that on a small mass of soot the available surface area could get coated with the organic acid early giving the first measurements a high uptake coefficient while little room left for additional acid later would give small uptake coefficients. A better evaluation was to compare different experiments of the same soot and organic acid combination. For this study, the masses used were either too close together for a trend to be observed or no clear trend was discernable. Figure 7 shows several uptake experiments of steric acid on activated propane soot. The mass of soot used was different for each experiment, and no trend between soot mass and uptake intensity was observed. These observations suggest that soot surface area was uniformly available throughout the soot mass, or that organic acid interaction with the soot was limited to the soot near the surface so the depth of the soot was irrelevant. In either case, it seems that the soot's physical or chemical makeup was more important than amount when considering uptake.

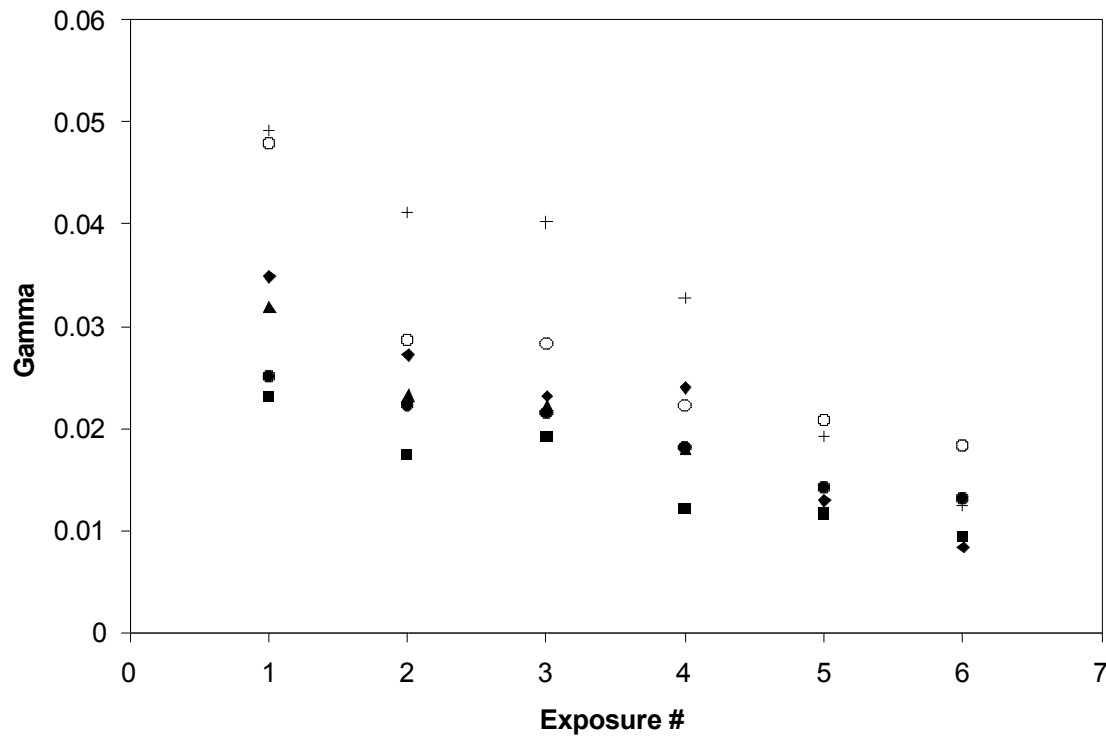


Figure 7. Comparison of uptake coefficients as a function of exposure number for steric acid uptake on different amounts of activated propane soot. Crosses, open circles, and diamonds represent masses 13.3, 18.0, and 47.7 mg respectively, while triangles, closed circles, and squares represent masses 21.7, 12.2, and 36.8 mg, respectively.

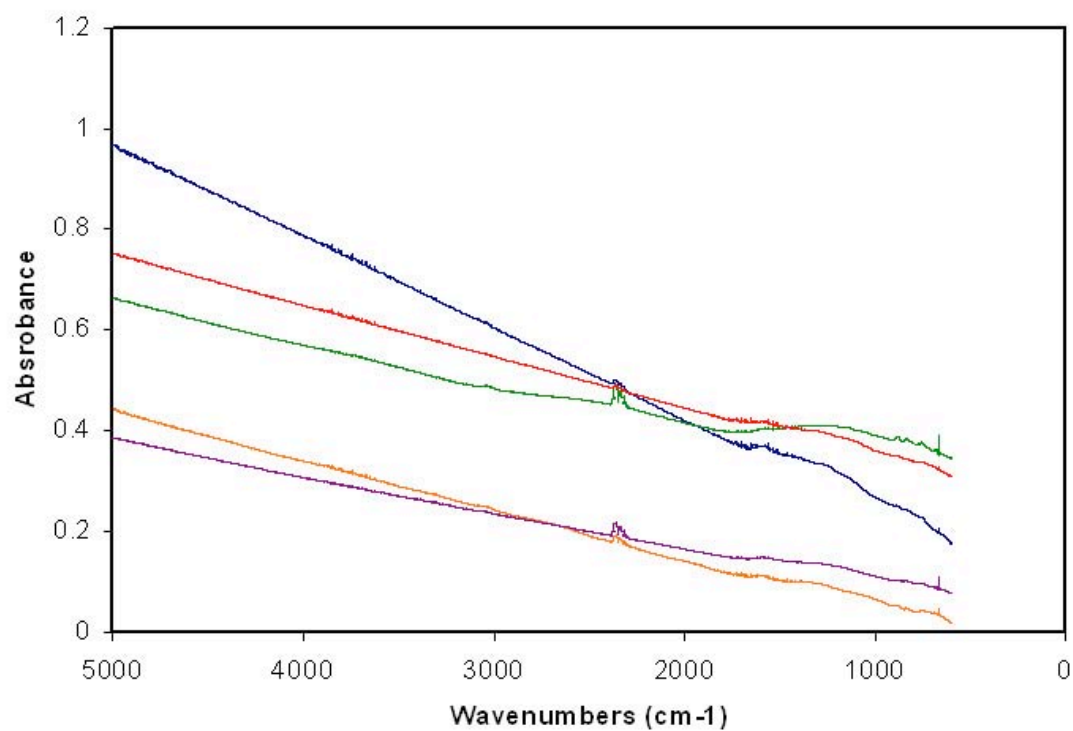


Figure 8. IR spectra of propane soot deposited on ZnSe crystal plates. The top three spectra are “activated” samples and the bottom two are “unactivated.” Spectra are shifted for clarity. Peaks located at ~ 2400 are due to CO_2 absorption in the gas phase.

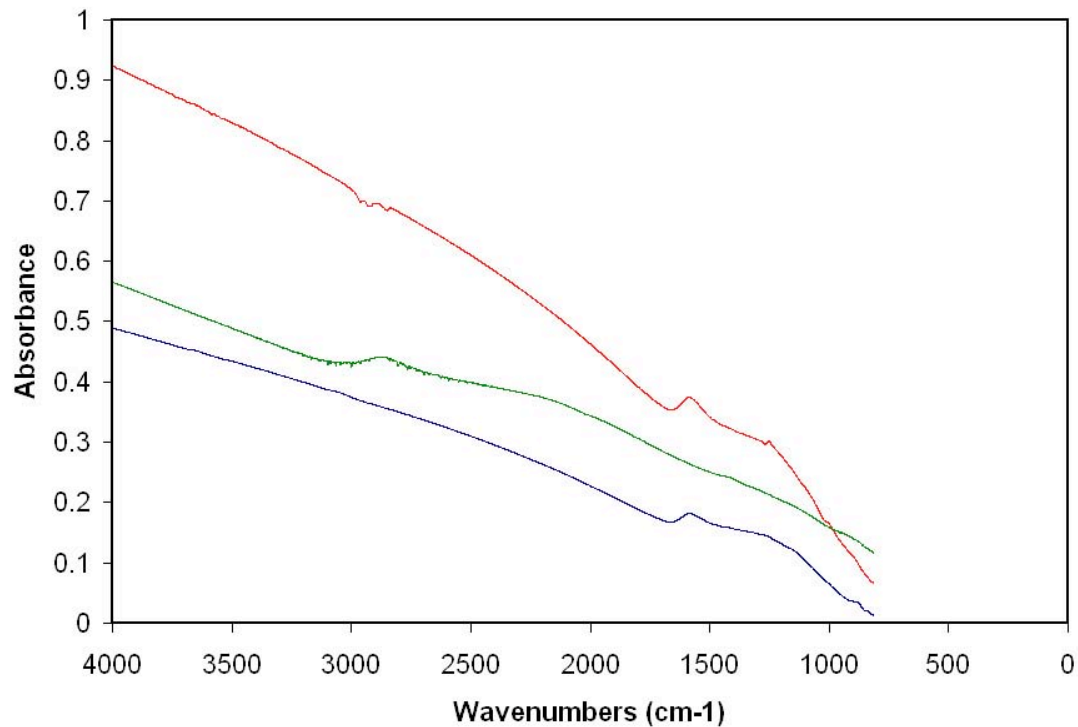


Figure 9. ATR and FTIR spectra of kerosene soot. The ATR is corrected for comparison to FTIR spectra and all spectra are shifted for clarity. The top spectrum is an ATR spectrum of “unactivated” soot and the bottom two are of “activated” soot. The green spectrum was taken by my FTIR instrument and the red and blue were collected with the ATR instrument.

3.2. Effect of Physical Properties on Uptake

As stated previously, soot mass contains approximately 10% oxygen and hydrogen, therefore FTIR spectroscopy as well as ATR-FTIR spectroscopy was employed to investigate any functional groups the oxygen and hydrogen constituency may comprise. This method also gives the added bonus of approximating the crystallinity and degree of order of the soot. FTIR alone allowed me to probe the bulk of the soot samples because IR-light was shone through the soot mass deposited on the ZnSe disk. ATR on the other hand is designed to allow interaction of the IR-light with only the first few micrometers of the subject's surface. Assuming the internal surface area of the soot was of similar chemical composition to the external surface area, the ATR method was more applicable to the present study because the uptake of organic acids on soot was most likely limited to surface interactions.

The investigation of bulk soot infrared absorption spectra did not indicate a significant amount of functionality. Figure 8 shows absorbance of propane soot over the wavelengths of 5000 to 750 cm^{-1} . The upper three spectra are of "activated" soot and the bottom two are "unactivated." The baselines are not corrected and the spectra are shifted for clarity. The slopes are slightly different for each case, likely due to variations in soot thickness, but are very similar otherwise. No clear functionality is observed in any of the FTIR spectra without baseline correction. For soot investigation with ATR spectroscopy very similar spectra were obtained. Figure 9 depicts "unactivated" (top) and "activated" (bottom two) kerosene soot spectra. Again baselines are uncorrected and shifted for clarity. As in the case of propane spectra, slopes vary slightly but

absorbance over the wavenumbers studied were very similar between “unactivated” samples and “activated” samples as well as between different types of soot or even the instrument collecting spectra. These methods were not able to identify any significant functional groups formed from oxygen in the soot that may facilitate uptake and were also not able to distinguish any significant chemical difference between soots produced from different fuels. From the investigation by FTIR and ATR no noticeable chemical difference between “unactivated” and “activated” soot exists. FTIR spectra for methane soot are also included in Figure 10. These spectra seem to have more functionality, but still their spectra were so similar to propane and kerosene, that it is unlikely uptake mechanism was different for methane soot.

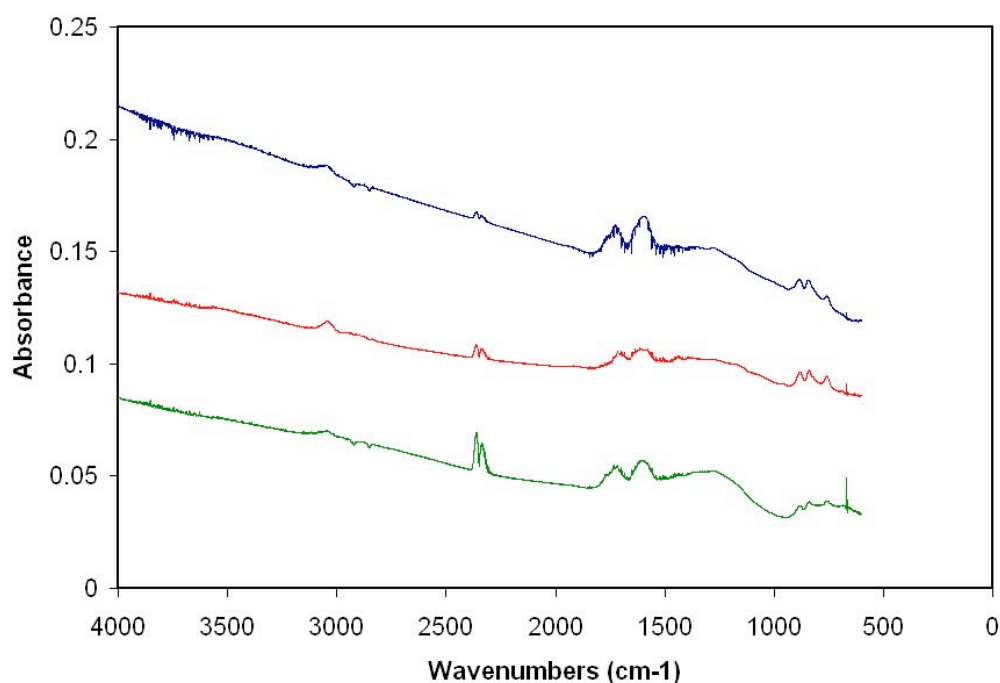


Figure 10. FTIR spectra of methane soot deposited on ZnSe crystal plates. All three spectra are “activated” samples. Spectra are shifted for clarity. Peaks located at ~ 2400 are due to CO_2 absorption in the gas phase.

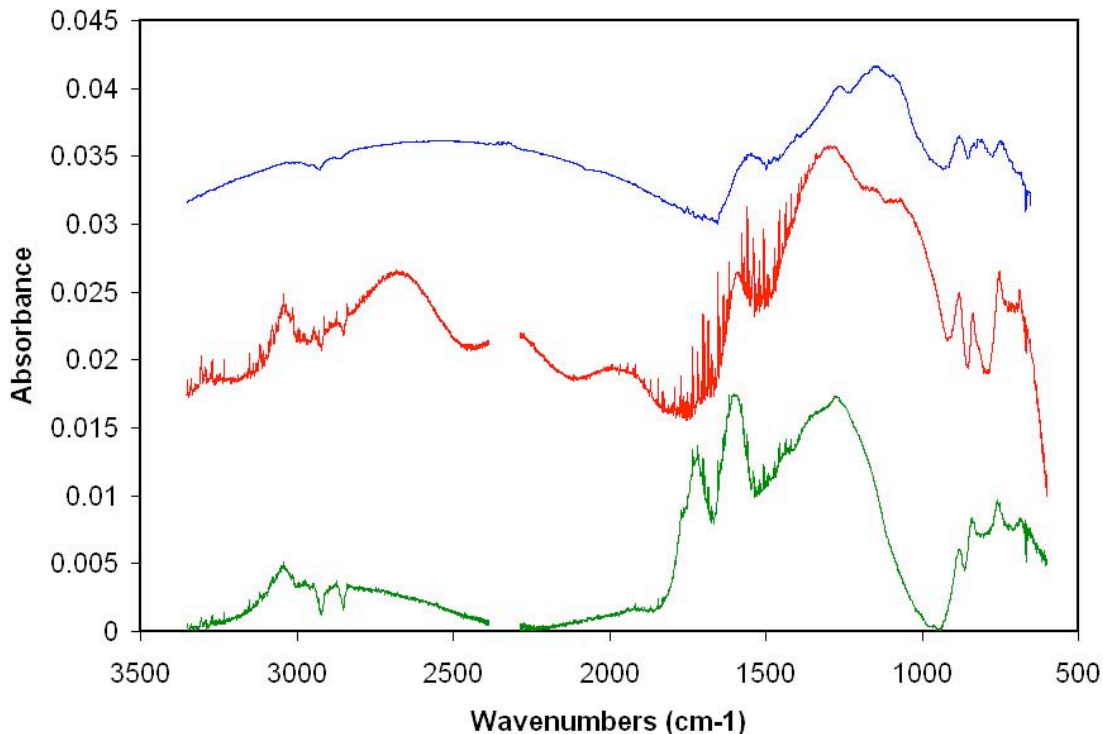


Figure 11. Baseline corrected spectra of activated kerosene soot collected by ATR (blue), activated propane soot (red), and methane soot (green). Spectra are shifted for clarity and the break in spectra between 2300 and 2390 cm^{-1} is a removal of gas phase CO_2 absorbance.

As stated previously, BC and EC can be organized in a variety of ordered or unordered arrangements. These structures range from highly crystalline to amorphous. Escribano et al. have employed Raman spectroscopy to study the degree of disorder of the carbon configuration in several types of carbon containing material.²⁹ Their investigation included multiple types of graphite as well as soots and ambient aerosols. Their results focused on four peaks in the Raman spectra located at 1350, 1575, 1600, and 2720 cm^{-1} . These peaks were identified as D, G, D', and 2D, respectively. The G peak was due to longitudinal symmetry axis C-C stretching of the graphite plane while

the other three were related to the crystallinity of the system. Figure 11 is of baseline corrected spectra found in Figures 8-10. Spectra are from top to bottom: “activated” kerosene soot collected by ATR, “activated” propane, and methane. The slightly shifted peaks in Figure 11 that correspond to D and G are located at 1300 and 1600 cm^{-1} , respectively. The D’ peaks are incorporated in the G peaks (as in Escribano et al.’s work). The 2D peaks are widely distributed in Figure 11 indicating absence of order in the soot structure. These peaks are centered at 2550, 2680, and 2820 cm^{-1} for kerosene, propane, and methane, respectively. Escribano et al. discovered that unless BC and EC had unorganized structure the D and D’ peaks were not present and when the G and D’ peaks merged forming one broad peak that a lack of three-dimensional ordering was present. It is clear from the weak but characteristic absorbance at these frequencies that the soots studied in this investigation were highly disordered. “Activated” soot samples were not significantly more ordered or disordered than “unactivated” samples, but due to peak widths and presence of other peaks it can be concluded that organization did vary slightly for soots from different fuel sources in this investigation.

Some functionality was also observed in the baseline corrected spectra. The peak in the propane and methane spectra at 3050 cm^{-1} was likely due to C-H stretch from the aromatic rings at the soot edges or possibly C-O-H functionality also at the surface. A C=O stretch may have been responsible for the peak in the methane soot spectra at 1730 cm^{-1} , this again would likely have been at the surface of the soot. Chughtai et al. have attributed absorbance at 1725 cm^{-1} to carboxylic species and used the peak to gauge oxidation of n-hexane soot.³² While the baseline corrected spectra do show some

evidence for oxygenated functionality, their weak absorbance compared to the uncorrected spectra, and the low A/F ratios used to produce the soot, likely limited their concentration and therefore their role in organic acid uptake.

To further characterize the physical properties of the soot as they pertain to organic acid uptake, I measured the surface area of each type of soot used for uptake experiments. The BET isotherm used to measure this quantity is similar to the Langmuir isotherm, but is able to account for multilayer adsorption of the condensing gas. Figure 12 is an example of a BET isotherm. Notice the large Kr uptake without any significant P/P_0 change at the beginning and end of the isotherm indicating a Type 2 isotherm.⁷⁵ As described in the Experimental section, the linear form of the BET equation can be plotted as P/P_0 vs. $P/[V(P_0-P)]$. An example of this can be seen in Figure 13 for the case of Kr adsorption on “unactivated” kerosene soot. The values determined by this method are given in Table 4. One set of values is listed for methane because soot deposition was not efficient enough if “unactivated” soot was collected. For the other two types of soot, the effect of “activating” the soot could be compared. The BET constant values found for the two propane cases were 70.06 for “unactivated” soot and 114.45 for “activated” soot. It is apparent from the table that “unactivated” propane soot had a larger surface area density than “activated” propane soot with 146.95 vs. 78.45 $\text{m}^2 \text{g}^{-1}$, respectively. This was also the case for kerosene soot, but the difference between the two was not as significant. “Unactivated” kerosene soot showed an average of 105.5 $\text{m}^2 \text{g}^{-1}$, while “activated” kerosene soot had the lowest surface area with 66.57 $\text{m}^2 \text{g}^{-1}$. The averaged BET constant values for “unactivated” and “activated” kerosene soot were 106.37 and

168.04, respectively. From the comparison of these two fuels, it seems “activation” of soot had a tendency to decrease the surface area of soot. Methane soot deposited in the “activated” manner averaged a surface area of $134.00 \text{ m}^2 \text{ g}^{-1}$ and had a BET constant of 32.66. One trend that arises from Table 4 is one of increasing surface area per mass with decreasing amount of soot used for the experiment. This was likely due to lower soot levels being increasingly less likely to be probed by Kr molecules. Aubin and Abbatt report that at a certain mass amount, surface area stopped growing with increasing soot amount for their BET investigations of n-hexane soot.⁴⁴ The surface area measured here for methane was higher than the values of up to $50 \text{ m}^2 \text{ g}^{-1}$ or more reported by Tesner and Shurupov.⁷⁶ My conditions were quite different from their heat induced pyrolysis and soot collection method, however. The value of kerosene BET surface area reported by Choi and Leu⁴⁹ of $91 \text{ m}^2 \text{ g}^{-1}$ falls between the values reported here for “unactivated” and “activated” kerosene soot. Ferry et al.³¹ report a BET surface area measured with Kr for kerosene soot to be $44 \text{ m}^2 \text{ g}^{-1}$. The soot amount used was over three times the average used during my experiments, which might help explain the difference. On the other hand, BET surface area found by a commercial instrument for kerosene was reported as $120 \pm 20 \text{ m}^2 \text{ g}^{-1}$ by Lelièvre et al.⁴⁶ The author is not aware of a published value for propane soot surface area.

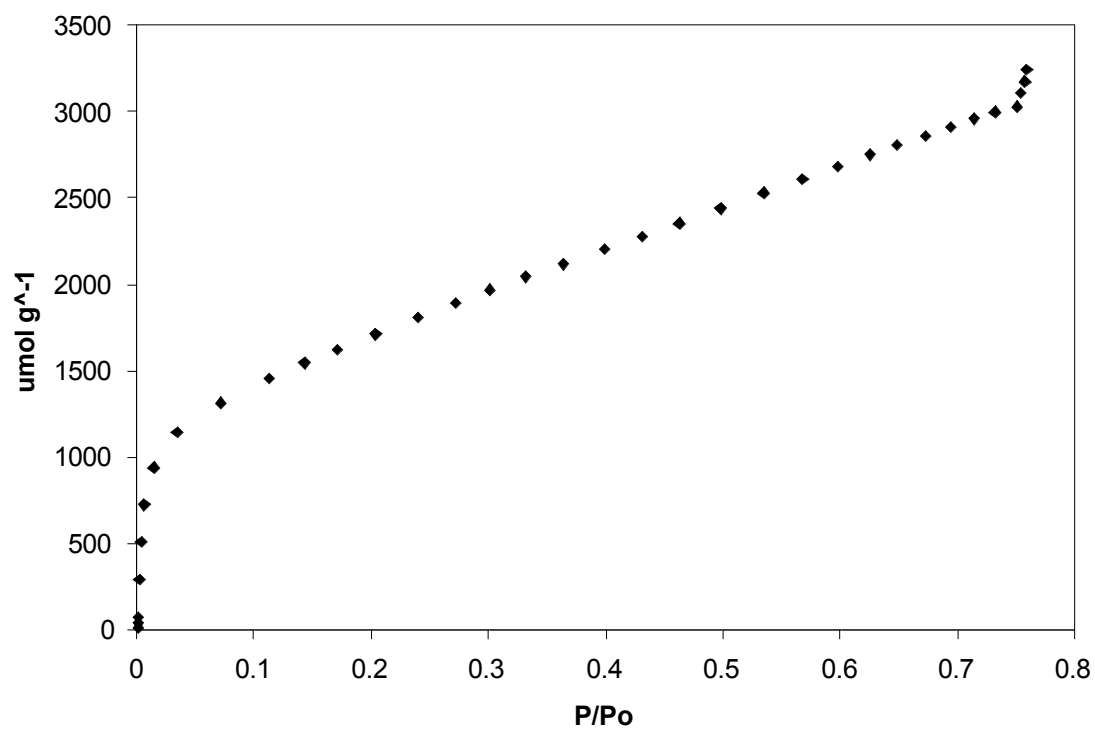


Figure 12. Adsorption isotherm of Kr on 0.0144 g of unactivated kerosene soot at 77.5 K.

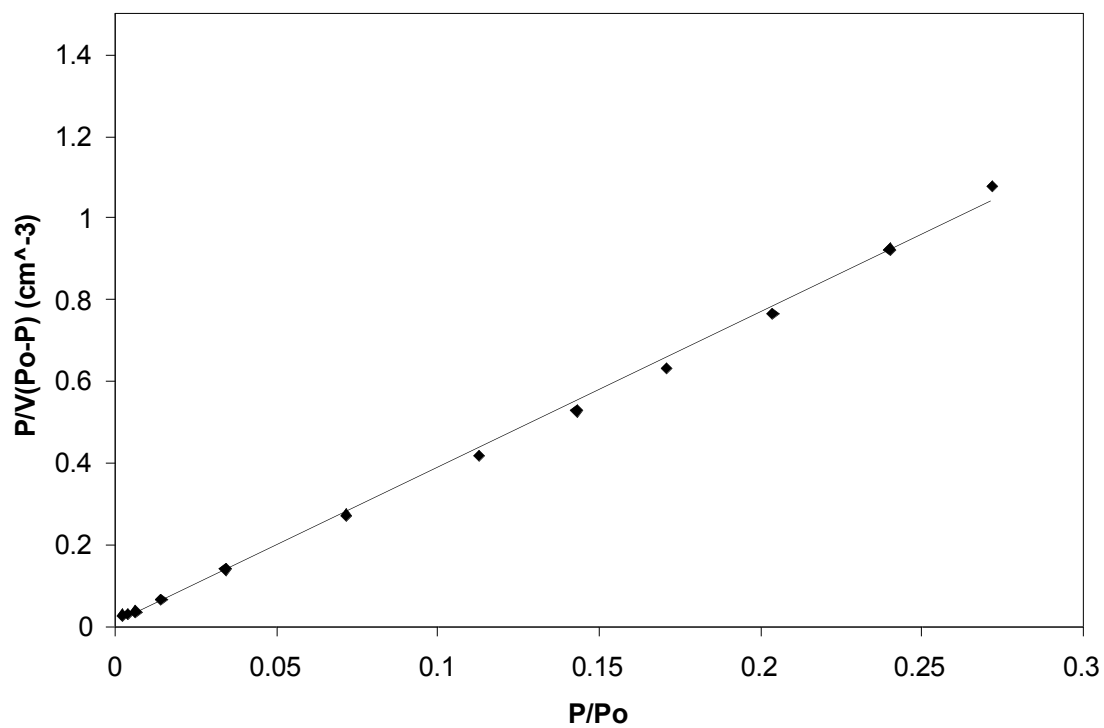


Figure 13. BET plot of $P/V(P_o-P)$ against P/P_o .

Table 4. BET Measured Soot Surface Areas

Experiment	Methane Surface Area ^a	Soot Mass ^b
1	174.85	3.7
2	112.42	8.3
3	114.41	9.4
4	160.24	5.0
5	108.10	18.0
Average	134.00 ± 31.13 ^c	8.9

Propane					
Experiment	Activated Surface Area	Soot Mass	Experiment	Unactivated Surface Area	Soot Mass
1	56.29	18.9	1	150.63	18.3
2	106.04	24.3	2	166.61	15.4
3	93.00	36.4	3	148.15	16.4
4	58.47	41.9	4	122.42	16.1
Average	78.45 ± 24.92	30.4	Average	146.95 ± 18.29	16.5

Kerosene					
Experiment	Activated Surface Area	Soot Mass	Experiment	Unactivated Surface Area	Soot Mass
1	75.26	16.9	1	98.30	14.4
2	68.93	69.0	2	92.75	19.1
3	81.40	63.6	3	133.25	5.6
4	48.69	190.2	4	97.51	28.9
5	58.58	115.9	5	93.67	59.6
6	n/a	n/a	6	112.05	44.5
Average	66.57 ± 13.08	91.1	Average	105.50 ± 18.70	28.7

^a Surface Areas are in units of m² g⁻¹.

^b Soot masses are in units of mg.

^c Error corresponds to unbiased second standard deviation (2σ).

Actual soot surface areas were much larger than the geometric surface area assumed when determining uptake coefficients. One uncertainty of this experimentation process is the amount of internal surface area available to the organic acids to deposit on. Using the soot surface areas listed in Table 4, the possible implication of increased surface area on uptake coefficients can be estimated. Total soot surface areas of the higher soot masses used in this study can have surface areas hundreds of times higher than the geometric surface area they occupy. Correspondingly, the uptake coefficients would be that many times lower if organic acids reached every possible square centimeter. This is highly unlikely, but certainly uptake coefficients given here represent an upper limit to atmospheric uptake and true coefficients are likely many times lower than those reported.

The effect of soot preparation, “unactivated” vs. “activated,” on uptake coefficients can further be considered as it relates to surface area. Table 2 can be consulted for this comparison for dicarboxylic acids while Table 3 is the source for monocarboxylic acid information. For propane, “activated” soot showed larger initial uptake than “unactivated” samples. For kerosene, a trend was not clear. Initial uptake values were very similar for oxalic, maleic, and glutaric acid on both kinds of soot. Phthalic acid uptake on “activated” kerosene soot had a large variability, so its comparison to “unactivated” experiments is not useful. Figures 14 and 15 show that for benzoic acid and steric acid on kerosene soot, respectively, the type of soot did not seem to affect the uptake. In the case of oleic acid uptake on propane however, uptake was higher on activated soot and the ranges of uncertainty between the two types did not

overlap. This can be seen graphically in Figure 16. This is contrary to what is expected when “activated” propane soot surface area is compared to “unactivated” propane soot surface area. A higher surface area per mass should have been able to accommodate a larger amount of organic acid. Steric acid uptake on the two propane soot types had overlapping error bars for the first four averages, but due to divergent uptake trends and decreasing variability, the last two averages did not overlap as seen in Figure 17. Uptake on activated propane soot was consistently higher, but this was possibly due to the greater soot masses and thus total surface areas used for those experiments. “Activated” kerosene soot masses used for benzoic acid uptake experiments were also larger than those of “unactivated” trials, but still the averaged values of “unactivated” soot uptake were generally higher. Considering the overlap of uncertainty for both soot types, it is hard to say if one uptake was truly higher than the other. It was also possible that because the “activated” and “unactivated” kerosene surface areas were relatively close the mass difference does not affect the uptake. The other two combinations had mass averages that were sufficiently similar enough for fair comparison. These findings generally agree with the report by Tesner and Polyakova that claim benzene has a significantly higher adsorption to channel black than lampblack.¹⁴

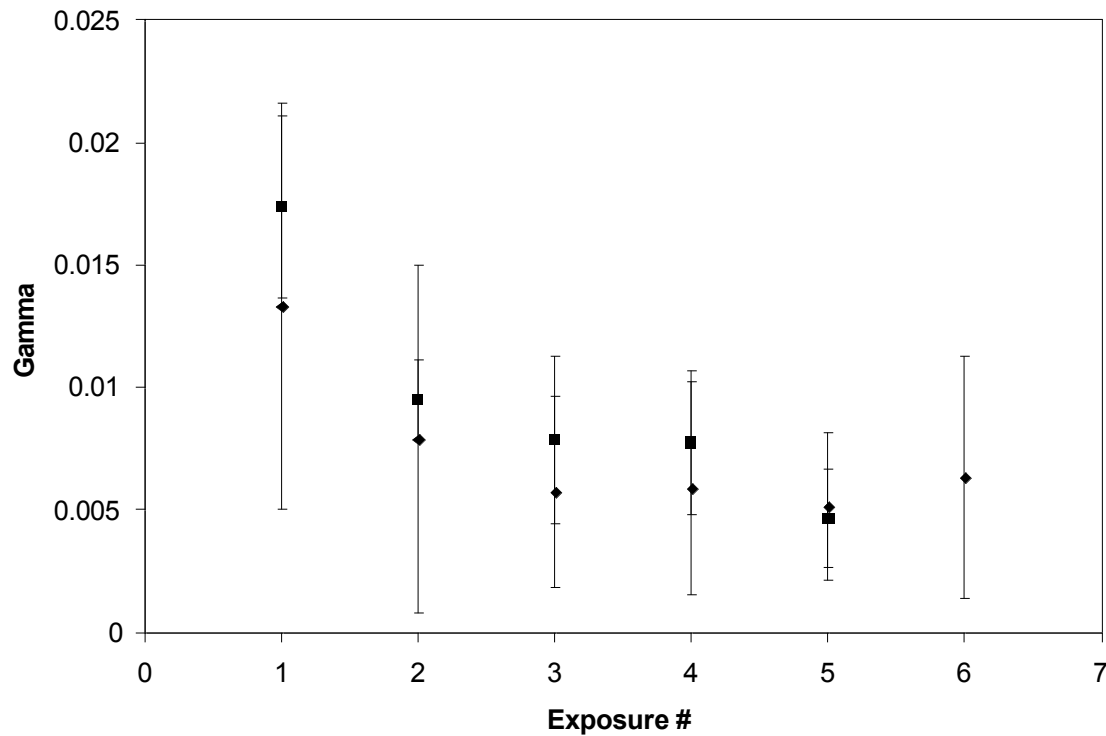


Figure 14. Uptake coefficients as a function of exposure number for benzoic acid uptake on kerosene soot. Solid squares identify “unactivated” data taken from Table 3 and solid diamonds are “activated” soot data taken from the same table. Error bars represent the standard deviation also given in Table 3.

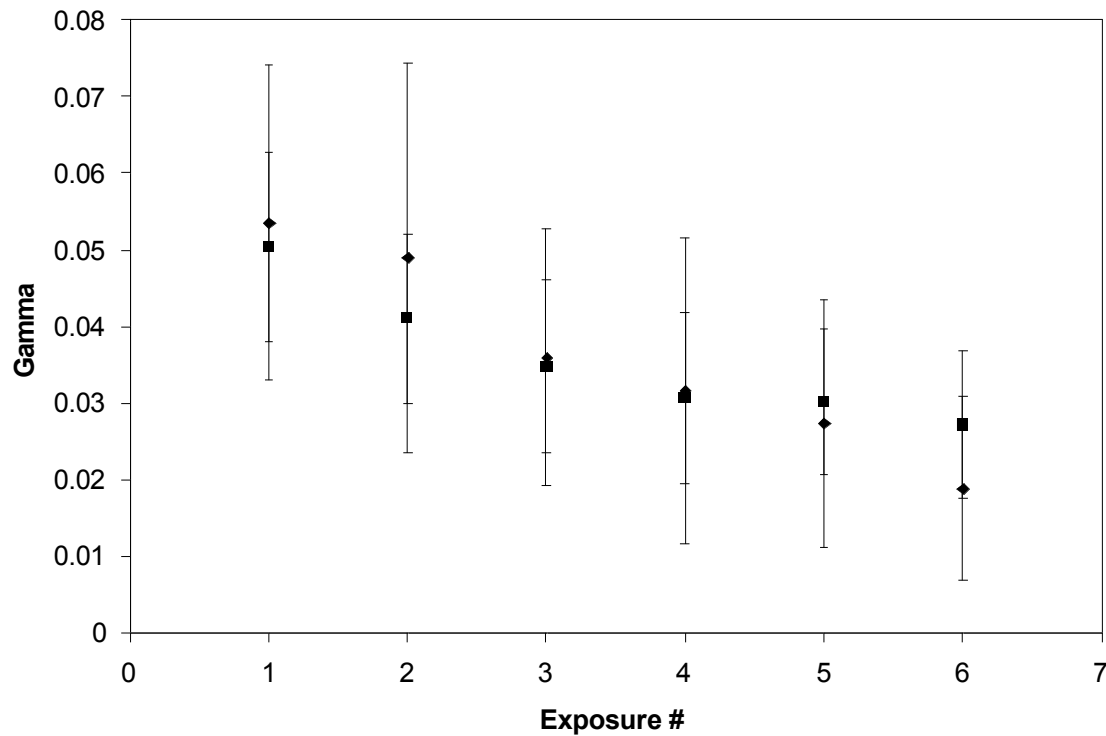


Figure 15. Uptake coefficients as a function of exposure number for Steric Acid uptake on kerosene soot. Solid squares identify “unactivated” data taken from Table 3 and solid diamonds are activated soot data taken from the same table. Error bars represent the standard deviation also given in Table 3.

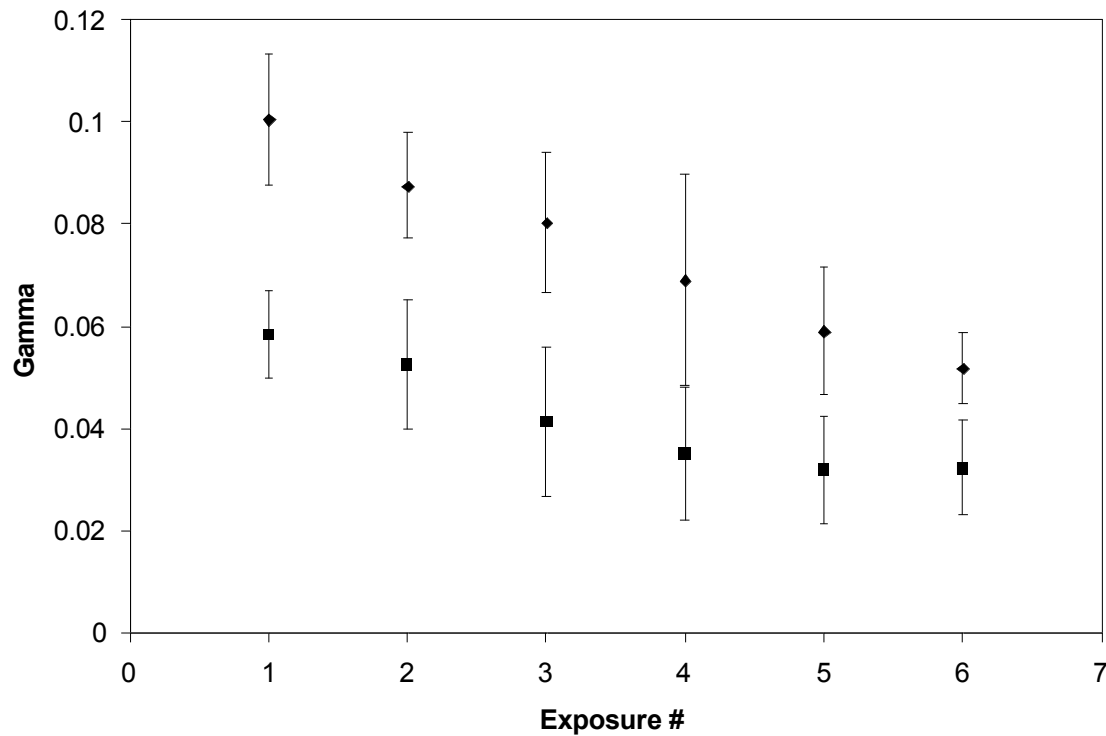


Figure 16. Uptake coefficient as a function of exposure number for oleic acid uptake on propane soot. Solid squares identify “unactivated” data taken from Table 3 and solid diamonds are “activated” soot data taken from the same table. Error bars represent the standard deviation also given in Table 3.

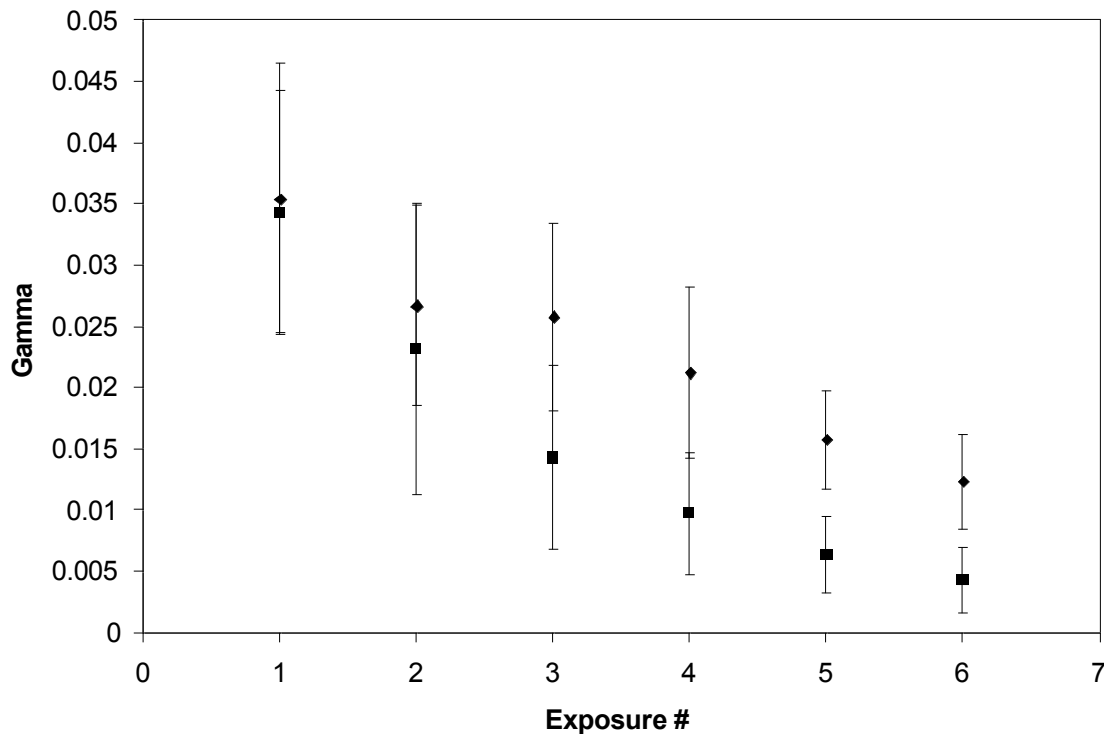


Figure 17. Uptake coefficient as a function of exposure number for steric acid uptake on propane soot. Solid squares identify “unactivated” data taken from Table 3 and solid diamonds are “activated” soot data taken from the same table. Error bars represent the standard deviation also given in Table 3.

For the cases that can be correlated to show larger uptake on “activated” soots, another physiochemical property must have been accountable. One property related to surface area is the porosity of the soot. Chughtai et al. have shown that soot surface area increased with increasing A/F ratios for n-hexane, JP-8 (jet fuel), and diesel fuel.³² Since surface area was affected by soot “activation” in this investigation, it is possible that the pore structure and connecting pore apertures could also have been affected by the soot “activation” process. While “activation” tended to decrease soot surface area,

this may have been due to opening and combining of internal pores. This decreased intricacy of the soot pore structure would have lead to lower surface area. Another property that may have been affected by soot deposition method was unpaired electron content. Chughtai et al. have also shown a linear relationship between unpaired electron spin density and A/F ratio,³² so it is possible that the deposition of soot in close proximity to the flames also had a similar effect. An increased concentration of unpaired electrons may have helped to increased uptake of organic acids like it did for small inorganic molecules.⁴⁵ In any case, it is likely soot “activation” had implications beyond changes in soot surface area.

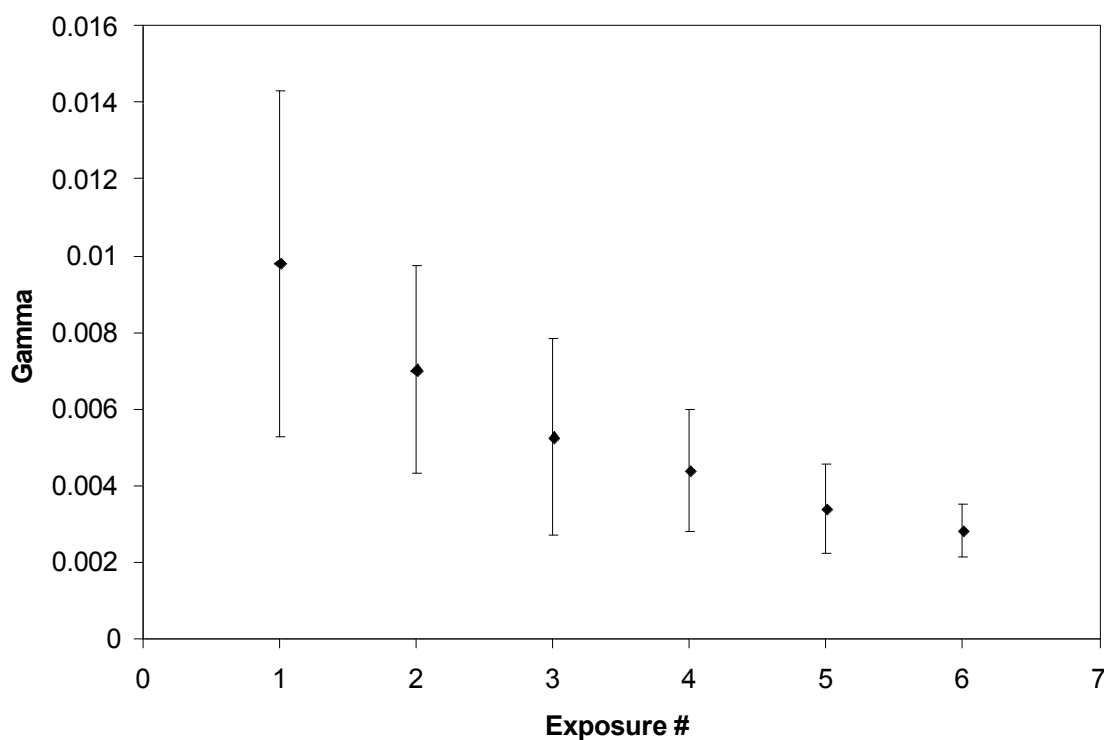


Figure 18. Uptake coefficients are displayed as a function of exposure number for steric acid uptake on methane soot. The uncertainty of the measurements decreases with progressive exposures.

One phenomenon worth consideration is the variability of the averaged uptake coefficients over exposure time length. For most monocarboxylic acid/soot combinations, the uncertainty in the uptake coefficient was significantly less for the sixth exposure than for the first. In many cases the error decreased with each exposure. This can be observed in Table 3 or Figures 14-17 but a lone example is graphically illustrated for better clarity in Figure 18 for steric acid uptake on methane soot. This trend may have been due to the scaling effect of decreasing uptake coefficient values, but it was not the case that the variability always decreased with the next exposure, so it is likely that there was a real activity or mechanism responsible. There was no correlation between average soot mass and decreasing variability, but there was for soot type and organic acid. Most of the combinations that did not follow this trend involve benzoic acid, kerosene soot, and soot that was unactivated. On the other hand, the factors that seem to have facilitated this trend were steric acid involvement, propane soot, and “activated” soot. The surface area relation propane soot and soot “activation” had may have been responsible for this trend, but the possibility of favorable interactions due to soot surface defects, the concentration of favorable uptake sites, or increased unpaired electron density may also explain why these two factors were associated with decreasing uptake variability with progressive exposures. Organic Acids may have penetrated into the soot mass during the first few exposures and could have blocked passages or adsorbed to those sites with the best conditions and effectively limited organic acid uptake area to the surface. Changes in blockage frequency during experimentation might have been facilitated by small changes in flow reactor pressure, gas velocity, or radial injector

position. Soot porosity and premium adsorption site number may also have changed depending on soot deposition conditions. Factors such as room air turbulence, flame size, and fuel flow may have changed from deposition to deposition to produce the sooting flame. With a more 2-dimensional uptake field and loss of a degree of freedom, the variability between experiments should have gone down. While steric acid and oleic acid have the same number of carbons in the carbon chain, the cis double bond in oleic acid makes it shorter, with more curvature in its structure. This more compact arrangement might make Oleic Acid potentially better able to penetrate into the soot mass while steric acid may not have fit into the soot as well. A related phenomenon has been observed by Kwon and Pignatello when studying benzene adsorption by charred maple wood shaving.⁷⁷ They found benzene adsorption at 293K was slightly depressed after char was exposed to vegetable oil, but N₂ BET isotherms at 77K showed significant decrease in internal surface area. Both observations were attributed to micropore throat blockage. Ferry et al. have used TEM imaging and adsorption isotherms to determine the diameters of nanotube-like pores in kerosene soot.³¹ They report diameters of a few to several nanometers wide and a theoretical estimation of steric acid and oleic acid molecular length of 2.1 and 1.5nm, respectively, puts these compounds at the lower end of this range. Optimized geometries of benzoic, steric and oleic acids are given in Figures 19, 20, and 21, respectively. Benzoic acid is obviously the shortest of the monocarboxylic acids studied at about 0.7 nm, but the length difference between steric acid and oleic acid is significant considering the only difference between their structures is merely one bond type. Figure 22 is of scaled cartoon representations of spherical soot

sub-particles, the nano-tube like throats between them, and rectangles that approximate 2-dimensional organic acids dimensions. If steric acid was more likely to block internal soot passages because it is longer, this might explain why it was associated with decreasing uptake variability with increasing previous exposure.

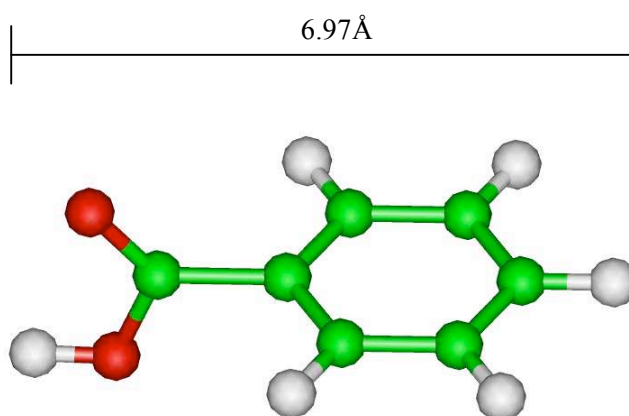


Figure 19. Theoretically optimized benzoic acid structure.

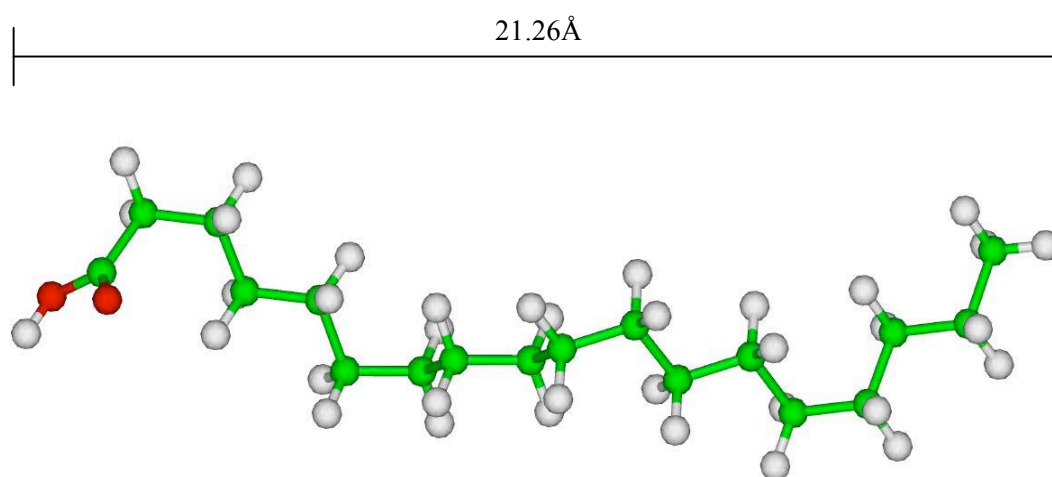


Figure 20. Theoretically optimized steric acid structure.

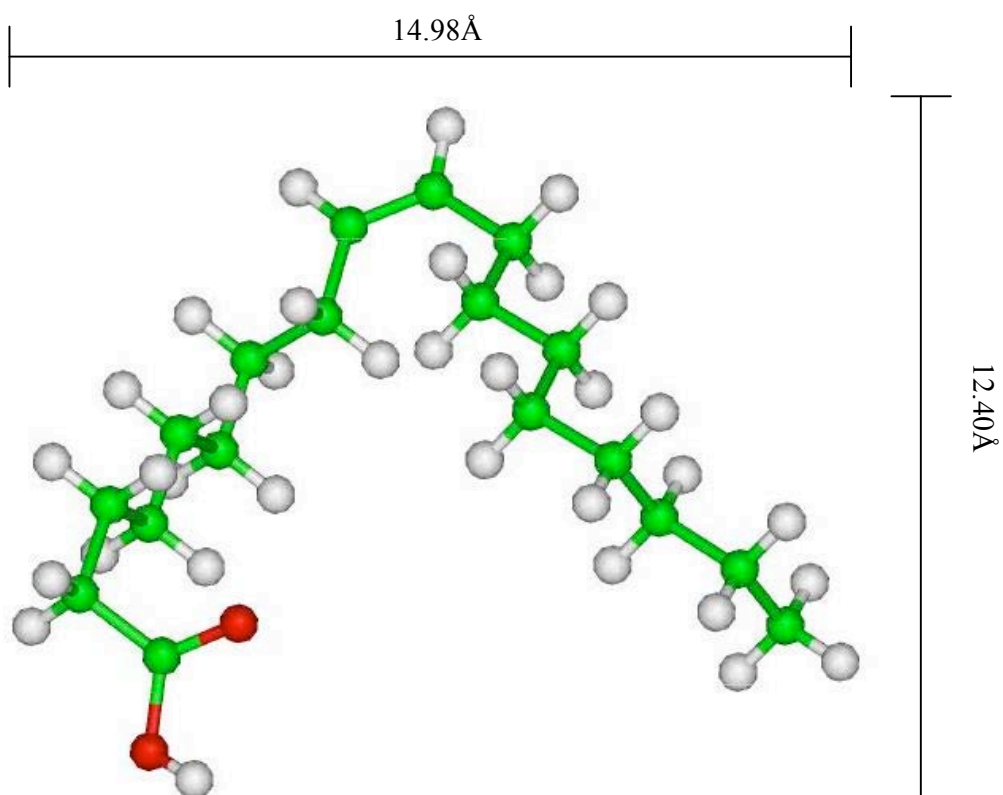


Figure 21. Theoretically optimized oleic acid structure.

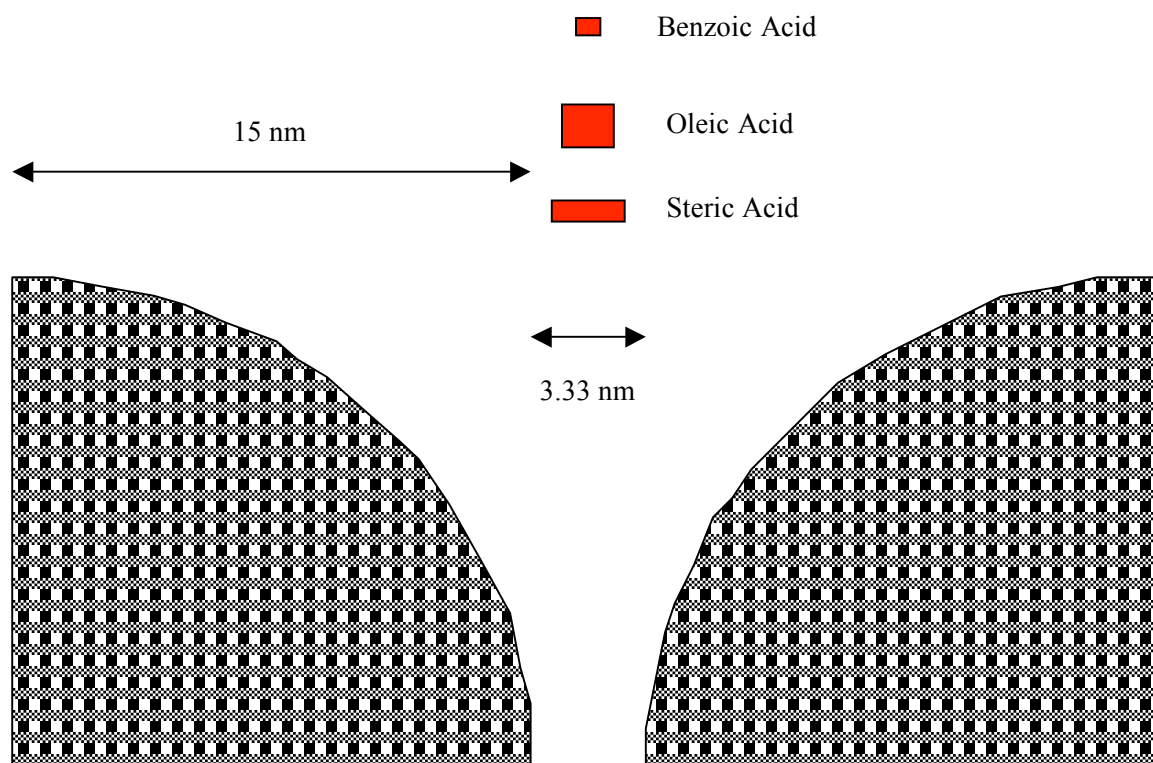


Figure 22. Cartoon representation of spherical soot sub-particles and organic acids to give an idea of scale.

To further assess the location of organic acid uptake and the extent to which organic acids partition to the internal surface area an estimation of the amount of monocarboxylic acids taken up by the different soot types has been made. While I was unable to measure the organic acid concentration in the flow tube with my methods, an estimation based on the organic acids' vapor pressures could be made. These estimations are given in Table 5. Using the estimated organic acid concentrations and experimental signal levels, the number of organic acid molecules lost to the soot surface was found. Next, an estimation of the monolayer surface area that the organic acids occupy was made. Coverage of total BET soot surface areas was very small (0.001-

0.04%) but if geometric surface area coverage was considered, the occupied space was more significant and also revealed more about uptake location. Geometric surface area coverage estimations are also given in Table 5. Benzoic acid values of 3-20% were too low to implicate uptake location, but the large oleic acid values, especially those over 100%, confirmed that this species (if not all) was able to adsorb to soot below the surface level. Benzoic acid coverages were likely related to its higher volatility and lower uptake coefficient. Steric acid geometric surface area coverage was on the low side with only a few percent, but this was likely due to its low concentration in the flow tube. It is likely that if oleic acid was able to adsorb on internal soot surfaces than the other organic acids were as well. The low coverage of steric acid on soot surfaces seems to conflict with the assessment that this molecule may be abundant enough on soot surfaces to block pore throats and thereby lower uptake variability. While the surface coverages presented in Table 5 are only estimations and cannot rule out pore blockage, they do suggest that uptake variability in the case of steric acid depended more on soot surface defects, favorable site conditions, or concentration of unpaired electrons and less on pore size or blockage.

Table 5. Estimated Organic Acid Coverage^a of Geometric Soot Surface

Soot Type		Methane	Propane		Kerosene	
			Unactivated	Activated	Unactivated	Activated
Acid	Conc. ^b					
Benzoic	1×10^{13}	3	N/A	11	16	20
Oleic	8×10^{12}	54	188	158	86	N/A
Steric	5×10^{11}	2	4	3	9	3

^a Coverage given as percentage

^b Estimated concentration in flow tube given in molecules cm⁻³

Ultimately, laboratory measurements are only as important as they are useful to further applications. For this reason, the data collected during experimentation was considered to gauge what extent organic acids can coat soot particles in the atmosphere. With a few basic assumptions, it was possible to estimate the time required to cover a given surface in a monolayer of organic acid. It is not clear how deep organic acids can penetrate into soot pores, so clear surface area availability was not apparent. Therefore it was useful to compare two approaches. For the first approach a spherical soot particle with 100 nm diameter was used. The second approach is similar to estimations made by Aubin and Abbatt⁴⁴ where $5 \times 10^{-12} \text{ g cm}^{-3}$ elemental carbon was considered available in an urban atmosphere.³⁰ For the spherical case, only the outer geometric surface was considered as the adsorbent surface. On the other hand, the surface areas presented in Table 4 were applied to the atmospheric mass densities and assuming a soot density of 2 g cm^{-3} a surface density on the order of $10^{-6} \text{ cm}^2 \text{ cm}^{-3}$ was found. Flux was calculated by mass transfer equations described by Seinfeld and Pandis³⁰ and both initially measured uptake coefficients as well as uptake coefficients on aged soot found in Table 3 were substituted for accommodation coefficients. Organic acid concentrations were conservatively estimated as 5 ppb. For the first method monolayer coverage was achieved very quickly ranging from 7 s for oleic acid on activated propane soot to 49 hours for benzoic acid on methane soot. With the second method, however, the fastest monolayer coverage was reached in 54 minutes by steric acid on activated kerosene soot while combinations of small uptake coefficients on large surface area soots took years to form a monolayer. Certainly actual monolayer coverage times are between these two

extremes, but clearly the amount of particulate surface area available for adsorption is vital to how important soot aging by organic acids is in the atmosphere.

4. CONCLUSIONS

In this work I have presented detailed descriptions of heterogeneous uptake of organic acids on “activated” methane soot and both “unactivated” and “activated” propane and kerosene soot at 296 K. Most carboxylic acids interacted with the different soot types by being irreversibly held; a few however were reversibly taken up or had no significant interaction. For the acids that showed irreversible uptake, the uptake coefficient (γ) was experimentally determined. Monocarboxylic acid uptake coefficients were collected for a series of exposures to gauge the “aging” effect. The uptake coefficient was found to vary widely depending on the fuel used to produce the soot and other factors. Chemical composition and surface areas of the soots were investigated to help understand factors affecting uptake.

Uptake of organic molecules on soot has been known to be driven by hydrogen bonding and van der Waals forces. Special $\pi - \pi$ interactions between unsaturated organic acid bonds and aromatic soot continuum is a recently studied phenomenon that also plays a role in the uptake this work was focused on. Previous experimental results of PAHs show that these interactions are reversible so it is unclear if and how these attractive forces are solely causing the irreversible uptake observed in my experiments.^{29,30} Dicarboxylic acids were not significantly less likely to show irreversible uptake than monocarboxylic acids, so carboxylic acid groups were likely participating in binding to soot surfaces. The oxygenated functional groups have not been studied in this light before and therefore their contribution is unclear. A recent soot structure investigation has shown that soot nanostructure may be less uniform than

graphite.⁷⁸ The new evidence shows small ring moieties that have higher hydrogen content and more molecular like character. It may be possible that these molecules within the soot superstructure also have functionality or unpaired electron density conducive to interaction with carboxylic acids. These dissimilar surface occurrences were possibly responsible for the difference in uptake and uptake variability among the experiments through changes in soot surface flaws or favorable uptake sight concentrations. More investigation is needed to determine the role oxygenated functional groups play in VOC adsorption to soot surfaces.

Initial uptake in the range of 9.0×10^{-4} to 7.7×10^{-3} was found for dicarboxylic acids. The uptake coefficients for monocarboxylic acids on a host of soot types measured in this study ranged from 1.4×10^{-3} to 1.0×10^{-1} over all conditions but also fluctuated within one subset of variables. Change within a subset was due to decreasing uptake after repeated exposures to the same soot sample. Uptake coefficient values generally decreased by half after six exposures, but more dramatic reductions were also observed. Decreasing uptake variability with increasing exposure could be related to the size of organic acids due to blockage of nanopores inside the soot structure or saturation of the favorable internal uptake sites forcing ensuing uptake to be limited to the surface. In either case, an estimation of the geometric soot surface coverage by dicarboxylic acids suggests uptake was not limited to the soot surface. For monocarboxylic acids the propane and kerosene fuels used to produce soot showed comparable uptake of organic acids, but methane soot showed consistently lower uptake coefficients. Oleic acid and steric acid had medium to high uptake in most cases while benzoic acid uptake was

lower on each type of soot. Maleic acid exhibited little or no irreversible uptake, but other dicarboxylic acids were lost to soot surfaces in roughly the same magnitude as monocarboxylic acids. The manner in which the soot was deposited also affected the uptake coefficients. “Activated” soot tends to facilitate slightly larger uptakes than “unactivated” soot possibly due to larger micropore throats, increased concentration of favorable uptake sites, or higher density of unpaired electrons.

To probe the effect chemical composition has on organic acid uptake, FTIR and ATR spectroscopy were employed. All soots exhibited similar absorption spectra suggesting functionality of soot was vastly sparse throughout the soot mass. These methods also showed that soot structure was highly unordered. Furthermore, no significant difference was observed between “unactivated” soot and “activated” soot by either of the two infrared methods. These results show another physical or chemical difference was accountable for variations in uptake intensities. BET adsorption isotherms measuring the surface area of soot samples were in the range of 66 to 146 m² g⁻¹. “Unactivated” soot samples showed larger surface areas than their “activated” counterparts. It is not clear why smaller surface areas would be conducive to greater uptake. Again, it is possible that soot “activation” caused another structural difference at the molecular or soot monomer unit level between the two types of soot undetectable by my methods.

Further investigation is needed to clarify binding mechanisms between oxygenated hydrocarbons and soot as well as the effect soot “activation” has on soot substructure. From my investigations, however, many organic acids have been shown to

have significant uptake interactions with common atmospheric soots. My results show this interaction may have implications for cloud microphysical properties, human health, radiative forcing, and global climate through alteration of the hygroscopic and optical properties of freshly formed soot aerosols.

REFERENCES AND NOTES

- (1) Yu, H.; Kaufman, Y. J.; Chin, M.; Feingold, G.; Remer, L. A.; Anderson, T. L.; Balkanski, Y.; Bellouin, N.; Boucher, O.; Christopher, S.; DeCola, P.; Kahn, R.; Koch, D.; Loeb, N.; Reddy, M. S.; Schulz, M.; Takemura, T.; Zhou, M. *Atmos. Chem. Phys.* **2006**, *6*, 613-666.
- (2) Lance, S.; Nenes, A.; Rissman, T. A. *J. Geophys. Res.* **2004**, *109*, D22208, doi:10.1029/2004JD004596.
- (3) Houghton, J. T.; Intergovernmental Panel on Climate Change. Working Group I. *Climate change 2001 : the scientific basis : contribution of Working Group I to the third assessment report of the Intergovernmental Panel on Climate Change*; Cambridge University Press: Cambridge, U.K., 2001.
- (4) Zhang, R. Y.; Suh, I.; Zhao, J.; Zhang, D.; Fortner, E. C.; Tie, X. X.; Molina, L. T.; Molina, M. J. *Science* **2004**, *304*, 1487-1490.
- (5) Penner, J. E.; Eddleman, H.; Novakov, T. *Atmos. Environ.* **1993**, *27*, 1277-1295.
- (6) Schultz, E. *Atmos. Environ.* **1993**, *27*, 1241-1249.
- (7) Gray, H. A.; Cass, G. R.; Huntzicker, J. J.; Heyerdahl, E. K.; Rau, J. A. *Sci. Total. Environ.* **1984**, *36*, 17-25.
- (8) Kaneyasu, N.; Murayama, S. *J. Geophys. Res.* **2000**, *105*, 19881-19890.
- (9) Mantell, C. L. *Carbon and graphite handbook*; Interscience Publishers: New York, 1968.
- (10) Mantell, C. L. *Industrial carbon : its elemental, adsorptive, and manufactured forms*, 2nd ed.; D. Van Nostrand: New York, 1946, p. 40-67, 72-73.
- (11) Donnet, J. B.; Voet, A. *Carbon black : physics, chemistry, and elastomer reinforcement*; M. Dekker: New York, 1976, p. 12-23, 70-81.
- (12) Beebe, R. A.; Polley, M. H.; Smith, W. R.; Wendell, C. B. *J. Am. Chem. Soc.* **1947**, *69*, 2294-2299.
- (13) Beebe, R. A.; Kington, G. L.; Polley, M. H.; Smith, W. R. *J. Am. Chem. Soc.* **1950**, *72*, 40-42.
- (14) Polyakova, M. M.; Tesner, P. A. *Dokl Akad Nauk Sssr* **1953**, *93*, 855-858.

- (15) Pidgeon, L. M. *Can. J. Res.* **1937**, *15B*, 187-207.
- (16) Avgul, N. N.; Kiselev, A. V. *Chemistry and physics of carbon* New York, M. Dekker, 1970; Vol. 6; pp 1-124.
- (17) Finlayson-Pitts, B. J.; Pitts, J. N. *Chemistry of the upper and lower atmosphere : theory, experiments, and applications*; Academic: San Diego, Calif., 2000, p. 326-328, 393-401.
- (18) Lawrence, J.; Koutrakis, P. *J. Geophys. Res.* **1996**, *101*, 9171-9184.
- (19) Peng, C.; Chan, M. N.; Chan, C. K. *Environ. Sci. Technol.* **2001**, *35*, 4495-4501.
- (20) Yao, X. H.; Fang, M.; Chan, C. K. *Atmos. Environ.* **2002**, *36*, 2099-2107.
- (21) Rogge, W. F.; Hildemann, L. M.; Mazurek, M. A.; Cass, G. R.; Simoneit, B. R. T. *Environ. Sci. Technol.* **1991**, *25*, 1112-1125.
- (22) Rogge, W. F.; Hildemann, L. M.; Mazurek, M. A.; Cass, G. R.; Simoneit, B. R. T. *Environ. Sci. Technol.* **1993**, *27*, 2700-2711.
- (23) Tervahattu, H.; Hartonen, K.; Kerminen, V. M.; Kupiainen, K.; Aarnio, P.; Koskentalo, T.; Tuck, A. F.; Vaida, V. *J. Geophys. Res.* **2002**, *107*, D16, doi:10.1029/2001JD001403.
- (24) Ellison, G. B.; Tuck, A. F.; Vaida, V. *J. Geophys. Res.* **1999**, *104*, 11633-11641.
- (25) Matsumoto, K.; Kawamura, K.; Uchida, M.; Shibata, Y.; Yoneda, M. *Geophys. Res. Lett.* **2001**, *28*, 4587-4590.
- (26) Fang, J. S. E.; Kawamura, K.; Ishimura, Y.; Matsumoto, K. *Environ. Sci. Technol.* **2002**, *36*, 2598-2604.
- (27) Mochida, M.; Kitamori, Y.; Kawamura, K.; Nojiri, Y.; Suzuki, K. *J. Geophys. Res.* **2002**, *107*, D17, doi:10.1029/2001JD001278.
- (28) Mansurov, Z. A. *Combust. Expl. Shock Waves* **2005**, *41*, 727-744.
- (29) Escribano, R.; Sloan, J. J.; Siddique, N.; Sze, N.; Dudev, T. *Vib. Spectrosc* **2001**, *26*, 179-186.

- (30) Seinfeld, J. H.; Pandis, S. N. *Atmospheric chemistry and physics : from air pollution to climate change*; Wiley: New York, 1998, P. 700.
- (31) Ferry, D.; Suzanne, J.; Nitsche, S.; Popovitcheva, O. B.; Shonija, N. K. *J. Geophys. Res.* **2002**, *107*, D23, doi:10.1029/2002JD002459.
- (32) Chughtai, A. R.; Kim, J. M.; Smith, D. M. *J. Atmos. Chem.* **2002**, *43*, 21-43.
- (33) Stanmore, B. R.; Brilhac, J. F.; Gilot, P. *Carbon* **2001**, *39*, 2247-2268.
- (34) Alcala-Jornod, C.; Rossi, M. J. *J. Phys. Chem. A* **2004**, *108*, 10667-10680.
- (35) Horvath, H. *Atmos. Environ.* **1993**, *27*, 293-317.
- (36) Schnaiter, M.; Horvath, H.; Mohler, O.; Naumann, K. H.; Saathoff, H.; Schock, O. W. *J. Aerosol Sci.* **2003**, *34*, 1421-1444.
- (37) Aubin, D. G.; Abbatt, J. P. *Environ. Sci. Technol.* **2006**, *40*, 179-187.
- (38) Kubicki, J. D. *Environ. Sci. Technol.* **2006**, *40*, 2298-2303.
- (39) Nguyen, T. H.; Ball, W. P. *Environ. Sci. Technol.* **2006**, *40*, 2958-2964.
- (40) Alcala-Jornod, C.; van den Bergh, H.; Rossi, M. J. *Phys. Chem. Chem. Phys.* **2000**, *2*, 5584-5593.
- (41) Zhang, D.; Zhang, R. Y. *Environ. Sci. Technol.* **2005**, *39*, 5722-5728.
- (42) Stier, P.; Seinfeld, J. H.; Kinne, S.; Feichter, J.; Boucher, O. *J. Geophys. Res.* **2006**, *111*, D18, doi:10.1029/2006JD007147.
- (43) Suzanne, J.; Ferry, D.; Popovitcheva, O.; Shonija, N. K. *Can. J. Phys.* **2003**, *81*, 423-429.
- (44) Aubin, D. G.; Abbatt, J. P. *J. Phys. Chem. A* **2003**, *107*, 11030-11037.
- (45) Chughtai, A. R.; Atteya, M. M. O.; Kim, J.; Konowalchuk, B. K.; Smith, D. M. *Carbon* **1998**, *36*, 1573-1589.
- (46) Lelievre, S.; Bedjanian, Y.; Pouvesle, N.; Delfau, J. L.; Vovelle, C.; Le Bras, G. *Phys. Chem. Chem. Phys.* **2004**, *6*, 1181-1191.

- (47) Longfellow, C. A.; Ravishankara, A. R.; Hanson, D. R. *J. Geophys. Res.* **2000**, *105*, 24345-24350.
- (48) Seisel, S.; Pashkova, A.; Lian, Y.; Zellner, R. *Faraday Discuss.* **2005**, *130*, 437-451.
- (49) Choi, W.; Leu, M. T. *J. Phys. Chem. A* **1998**, *102*, 7618-7630.
- (50) Kirchner, U.; Scheer, V.; Vogt, R. *J. Phys. Chem. A* **2000**, *104*, 8908-8915.
- (51) Prince, A. P.; Wade, J. L.; Grassian, V. H.; Kleiber, P. D.; Young, M. A. *Atmos. Environ.* **2002**, *36*, 5729-5740.
- (52) Longfellow, C. A.; Ravishankara, A. R.; Hanson, D. R. *J. Geophys. Res.* **1999**, *104*, 13833-13840.
- (53) Al-Abadleh, H. A.; Grassian, V. H. *J. Phys. Chem. A* **2000**, *104*, 11926-11933.
- (54) Korfmacher, W. A.; Wehry, E. L.; Mamantov, G.; Natusch, D. F. S. *Environ. Sci. Technol.* **1980**, *14*, 1094-1099.
- (55) Yang, K.; Zhu, L. Z.; Xing, B. S. *Environ. Sci. Technol.* **2006**, *40*, 1855-1861.
- (56) Zhu, D. Q.; Kwon, S.; Pignatello, J. J. *Environ. Sci. Technol.* **2005**, *39*, 3990-3998.
- (57) Mikhailov, E. F.; Vlasenko, S. S.; Podgorny, I. A.; Ramanathan, V.; Corrigan, C. E. *J. Geophys. Res.* **2006**, *111*, D7, doi:10.1029/2005JD006389.
- (58) Zhao, J.; Levitt, N. P.; Zhang, R. Y. *Geophys. Res. Lett.* **2005**, *32*, L09802, doi:10.1029/2004GL022200.
- (59) Levitt, N. P.; Zhao, J.; Zhang, R. Y. *J. Phys. Chem. A* **2006**, *110*, 13215-13220.
- (60) Zhao, J.; Levitt, N. P.; Zhang, R. Y.; Chen, J. M. *Environ. Sci. Technol.* **2006**, *40*, 7682-7687.
- (61) Jones, C. C.; Chughtai, A. R.; Murugaverl, B.; Smith, D. M. *Carbon* **2004**, *42*, 2471-2484.

- (62) Fortner, E. C.; Zhao, J.; Zhang, R. Y. *Anal. Chem.* **2004**, 76, 5436-5440.
- (63) Keyser, L. F.; Moore, S. B.; Leu, M. T. *J. Phys. Chem.* **1991**, 95, 5496-5502.
- (64) Zhang, R. Y.; Jayne, J. T.; Molina, M. J. *J. Phys. Chem.* **1994**, 98, 867-874.
- (65) Zhang, R. Y.; Leu, M. T.; Keyser, L. F. *J. Phys. Chem.* **1994**, 98, 13563-13574.
- (66) Brown, R. L. *J. Res. Natl. Bur. Stand. (U.S.)* **1978**, 83, 1-8.
- (67) Fuller, E. N.; Schettle, P. D.; Giddings, J. C. *Ind. Eng. Chem.* **1966**, 58, 19-&.
- (68) Marrero, T. R.; Luecke, R. H. *Aiche Journal* **1996**, 42, 2365-2368.
- (69) Brunauer, S.; Emmett, P. H.; Teller, E. *J. Am. Chem. Soc.* **1938**, 60, 309-319.
- (70) Rosenberg, A. J. *J. Am. Chem. Soc.* **1956**, 78, 2929-2934.
- (71) Gregg, S. J.; Sing, K. S. W. *Adsorption, surface area, and porosity*, 2nd ed.; Academic Press: New York, 1982, p. 1-190.
- (72) Sing, K. S. W.; Everett, D. H.; Haul, R. A. W.; Moscou, L.; Pierotti, R. A.; Rouquerol, J.; Siemieniewska, T. *Pure Appl. Chem.* **1985**, 57, 603-619.
- (73) Keyser, L. F.; Leu, M. T. *J. Colloid Interface Sci.* **1993**, 155, 137-145.
- (74) Zhang, R. Y.; Leu, M. T.; Keyser, L. F. *J. Geophys. Res.* **1995**, 100, 18845-18854.
- (75) Brunauer, S.; Deming, L. S.; Deming, W. E.; Teller, E. *J. Am. Chem. Soc.* **1940**, 62, 1723-1732.
- (76) Tesner, P. A.; Shurupov, S. V. *Combust. Sci. Technol.* **1995**, 109, 399-400.
- (77) Kwon, S.; Pignatello, J. J. *Environ. Sci. Technol.* **2005**, 39, 7932-7939.
- (78) Kis, V. K.; Posfai, M.; Labar, J. L. *Atmos. Environ.* **2006**, 40, 5533-5542.

VITA

Name: Nicholas Paul Levitt

Address: 11435 Rebecca Creek Rd
Spring Branch, Tx 78070

Email Address: nlevitt45@yahoo.com

Education: B.S., Chemistry, Texas A&M University, 2004